THE JOURNAL OF BIOLOGICAL CHEMISTRY VOL. 290, NO. 9, pp. 5311–5327, February 27, 2015

The Na^+/H^+ Exchanger NHE6 Modulates Endosomal pH to Control Processing of Amyloid Precursor Protein in a Cell Culture Model of Alzheimer Disease*

Received for publication, August 4, 2014, and in revised form, December 29, 2014 Published, JBC Papers in Press, January 5, 2015, DOI 10.1074/jbc.M114.602219

Hari Prasad[1] **and Rajini Rao**[2]

From the Department of Physiology, The Johns Hopkins University School of Medicine, Baltimore, Maryland 21205

Background: NHE6 transports protons out of the endosomal lumen in exchange for cations.
Results: Localization and processing of amyloid precursor protein are altered by NHE6 expression.
Conclusion: NHE6 controls Aβ production and is down-regulated in Alzheimer disease brains.
Significance: NHE6 and related orthologs may be risk factors for Alzheimer disease.

Early intervention may be key to safe and effective therapies in patients with Alzheimer disease. Endosomal dysfunction is an early step in neurodegeneration. Endosomes are a major site of production of Aβ peptide from the processing of amyloid precursor protein (APP) by clipping enzymes (β- and γ-secretases). The β-secretase enzyme BACE1 requires acidic lumen pH for optimum function, and acid pH promotes Aβ aggregation. The Na^+/H^+ exchanger NHE6 provides a leak pathway for protons, limiting luminal acidification by proton pumps. Like APP, NHE6 expression was induced upon differentiation of SH-SY5Y neuroblastoma cells and localized to an endosomal compartment. Therefore, we investigated whether NHE6 expression altered APP localization and processing in a stably transfected cell culture model of human APP expression. We show that co-expression with NHE6 or treatment with the Na^+/H^+ ionophore monensin shifted APP away from the *trans*-Golgi network into early and recycling endosomes in HEK293 cells. NHE6 alkalinized the endosomal lumen, similar to monensin, and significantly attenuated APP processing and Aβ secretion. In contrast, Aβ production was elevated upon NHE6 knockdown. We show that NHE6 transcript and protein levels are lowered in Alzheimer brains relative to control. These findings, taken together with emerging genetic evidence linking endosomal Na^+/H^+ exchangers with Alzheimer disease, suggest that proton leak pathways may regulate Aβ generation and contribute to disease etiology.

NHE6 is an isoform of the superfamily of Na^+/H^+ exchangers, localizing to early and recycling endosomes, where it exchanges luminal H^+ for cations (Na^+ or K^+) (1, 2). Endosomal pH is precisely tuned by a combination of inward proton pumping through V-ATPase and outward proton leak via endosomal $Na^+(K^+)/H^+$ exchangers, both mechanisms that are evolutionarily conserved from yeast to plants, fruit fly, and mammals (3). Loss-of-function mutations in endosomal $Na^+(K^+)/H^+$ exchangers cause hyperacidification of the endosomal lumen, as a result of imbalance in the pump and leak pathways. In the budding yeast *Saccharomyces cerevisiae*, deletion of the endosomal $Na^+(K^+)/H^+$ exchanger ortholog Nhx1/Vps44 leads to cellular phenotypes reminiscent of early stages of Alzheimer disease: enlargement of endosomal compartments, enhanced proteolysis of the chaperone protein Vps10 (a homolog of the AD[3] susceptibility factor SORL1), and profound deficiencies in protein sorting and lysosomal cargo delivery that also characterize neurodegeneration (3–5). These cellular phenotypes were linked to luminal pH; we showed that trafficking defects could be mimicked by weak acids or corrected in *nhx1*Δ mutants with weak base (3). Furthermore, in a genome-wide analysis of vacuolar pH in ~4,600 yeast null mutants, we observed a link between dysregulation of luminal pH and vesicle trafficking (6).

Enlarged endosomes are the earliest neuronal pathology described in AD, and recent intriguing studies have implicated endocytic dysfunction, perturbations of vesicle trafficking, and lysosomal pH deficits in the mechanism of neurodegeneration (7, 8). Several genes identified in genome-wide association studies of AD risk, including *BIN1*, *PICALM*, *CD2AP*, *EPHA1*, and *SORL1*, are known to be involved in endosomal mechanisms (9). Amyloid precursor protein APP, its proteolytic fragments (Aβ and βCTF), and key processing enzymes (β-APP cleavage enzyme BACE1; γ-secretase) localize to endosomes, linking APP processing to endosome function. The acidic pH of the endosomal lumen is pre-requisite and essential to amyloid pathology in at least four different ways: thus, (i) the obligatory and rate-limiting convergence of APP/BACE-1 (substrate/enzyme) vesicles in neurons has been shown to be acid-pH dependent, (ii) as is the pH optimum of the BACE-1 protease (10, 11). Lowering BACE-1 levels reduces neurodegeneration and behavioral defects in APP transgenic mice, pointing to its importance as therapeutic target (12). Furthermore, (iii) the protonation states of the three histidine residues in Ab (His6, His13 and His14) have been reported to promote aggregation

* This work was supported, in whole or in part, by National Institutes of Health Grants DK054214 and GM62142 (to R. R.).
[1] A Fulbright Fellow supported by the International Fulbright Science and Technology Award.
[2] To whom correspondence should be addressed: Dept. of Physiology, 725 N. Wolfe St., Baltimore, MD 21205. E-mail: rrao@jhmi.edu.

[3] The abbreviations used are: AD, Alzheimer disease; APP, amyloid precursor protein; TGN, *trans*-Golgi network; Tfn, transferrin; MMSE, mini-mental state examination; CTX, cortex; BA, Brodmann area.

via pH-dependent effect on the formation of b-sheets and the binding of metal ions to Ab (13). Most recently, (iv) acidic luminal pH has been shown to attenuate lysosomal degradation of Ab by disrupting SORLA-Ab interaction (14). These observations suggest that modulation of luminal pH by endosomal NHE activity may offer novel strategies to control APP trafficking and processing.

SLC9A6, the gene encoding NHE6, is one of the six most recurrently mutated loci in patients with X-linked intellectual disability and has been linked to autism comorbid with seizures, Christianson syndrome, and Angelman-like syndrome (15–19). Autism spectrum disorder has emerged as a major public health concern worldwide with an urgent unmet need for effective and safe interventions (1). With an aging population, Alzheimer and related neurodegenerative disorders pose a similar challenge (20). Interestingly, the Aβ and Tau pathologies linked by the amyloid cascade hypothesis have been implicated in autism, Fragile X syndrome, and 15q duplication in patients and animal models (21–23). These recent revelations about the shared pathology of altered processing of amyloid precursor protein (APP) between autism spectrum disorder and Alzheimer disease may point the way to new treatments. Indeed, histopathological examination of post-mortem brain tissue from patients with NHE6 mutations shows widespread neuronal loss, gliosis, and deposits of the hyperphosphorylated microtubule binding protein Tau in tangles and inclusions in neurons and glia (18). Research showing NHE6 down-regulation in substantia nigra in patients with Parkinson disease further signifies an emerging role for endosomal pH and NHE6 activity in the underlying mechanisms of neurodegeneration (24). Finally, closely related NHE6 paralogs have also been implicated in AD in genome-wide association studies (25, 26).

In this study, we examine the relationship between NHE6 and APP in human brains, differentiated neuroblastoma cells in culture, and an AD model of stable human APP expression in HEK293 cells. We show that NHE6 expression is linked to APP and other early onset Alzheimer risk genes. In cultured cells, NHE6 colocalizes with and alters processing of APP by modulating endosomal pH. Together with reduced protein levels of NHE6 in AD brains, our findings suggest that endosomal pH modulation by Na^+/H^+ exchangers may be an important factor in neurodegenerative disease.

EXPERIMENTAL PROCEDURES

Cell Culture—Human neuroblastoma SH-SY5Y cells (gift from Dr. Svetlana Lutsenko, Johns Hopkins University) were maintained in minimal essential medium/F-12 supplemented with 10% FBS (Invitrogen). Neuronal differentiation of SH-SY5Y was induced as described earlier (27). Briefly, cells were sequentially treated with 10 nM retinoic acid (Sigma) for 5 days and 50 ng/ml brain-derived neurotrophic factor (Shenandoah Biotechnology) in serum-free medium for the subsequent 3 days. Stable HEK293 cells expressing human APP695 (gift from Dr. Randy Schekman, University of California, Berkeley, CA) were cultured in DMEM/high glucose/sodium pyruvate (Invitrogen) with the addition of 10% FBS (Invitrogen), Glutamax (Invitrogen), NEAA (Quality Biological), 650 μg/ml Geneticin/G418 (Corning Cellgro) and maintained in a humidified incubator with 5% CO_2 at 37 °C. NHE6-GFP and control vector (GFP) expression were introduced using lentiviral packaging and expression, as described earlier (28). For transferrin uptake and endosomal pH measurement experiments, to avoid spectral overlap with Alexa Fluor 488 or FITC-tagged transferrin, we expressed NHE6 (wild type and mutant) tagged to C-terminal mCherry in HEK293 cells by transient transfection using Lipofectamine 2000 reagent, as per the manufacturer's instructions. Cell viability was measured using the trypan blue exclusion method. Briefly, cells were mixed 1:1 in suspension with a 0.4% solution of trypan blue Stain. A 10-μl sample was added to a disposable cell counting chamber slide and inserted into a Countess automated cell counter (Invitrogen). The cell viability and total cell numbers were recorded from six independent experiments, as described earlier (29).

Antibodies—Mouse monoclonal antibodies used were anti-EEA1 (catalog no. 610456, BD Transduction Laboratories), Rab11 (catalog no. 610656, BD Transduction Laboratories), anti-Golgin 97 (CDF4, Invitrogen), and anti-Aβ1–16 (6E10, Signet/Covance). Rabbit monoclonal BACE antibody was purchased from Cell Signaling (catalog no. 5606, D10E5). mCherry rat monoclonal antibody was obtained from Invitrogen (catalog no. M11217). Specific rabbit polyclonal NHE6 antibody was raised against the C terminus of NHE6. Rabbit polyclonal anti-APP C-terminal antibody was obtained from Sigma. Monoclonal mouse β-amyloid antibody (G48) was kindly provided by Dr. Philip Wong (Johns Hopkins University). Mouse polyclonal Arc antibody was a kind gift from Dr. Paul Worley (Johns Hopkins University).

Plasmids—Human NHE6-EGFP was cloned into FUGW-lentiviral vector into the BamHI site. NHE6 was cloned into mCherry pcDNA3 vector using HindIII and EcoRI sites to yield NHE6-mCherry construct. A QuikChange Lightning site-directed mutagenesis kit was used to engineer ΔWST^{372} in-frame deletion into NHE6. The resulting plasmid was confirmed by sequencing. Mouse BACE1 plasmid developed by the Thinakaran laboratory was obtained from Addgene (plasmid 26736). This construct has a C-terminal FLAG tag and engineered mutations, previously shown to neither alter localization nor function of BACE1 (30). HsNHE6 short hairpin RNA (shRNA) sequence (5′-CCGGCGTCCTAGTGCATGTCTCTGTTCAAGAGACAGAGACATGCACTAGGACTTTTTC-3′) was designed to target the 3′-untranslated region (3′-UTR). Both HsNHE6 shRNA and scrambled control construct were cloned into pLKO.1 lentiviral vector with a puromycin-selectable marker.

Western Blotting and ELISA—Human brain tissue was obtained from the Johns Hopkins Brain Bank and used in accordance with institutional guidelines. For Western blots, samples of medial frontal cortex gray matter were obtained by punch biopsy and dissolved in 1% Triton and 0.2% SDS lysis buffer. For Western blots of cell culture lysate, cells were lysed using Nonidet P-40 (1%) supplemented with protease inhibitor mixture (Roche Applied Science). Cells were sonicated, and the protein concentration was determined by a BCA assay. Equal amounts of proteins were separated by SDS-PAGE under reducing conditions and then electrophoretically transferred onto nitrocellulose membranes (Bio-Rad). After protein transfer, the membranes were treated with the blocking buffer, fol-

lowed by incubations with primary antibodies and then with HRP-conjugated secondary antibodies (GE Healthcare). Super-Signal West Pico substrate was used for detection. Fujifilm LAS 3000 imaging system was used to capture images. Tubulin or glyceraldehyde-3-phosphate dehydrogenase (GAPDH) was used as a loading control. For quantification of Aβ40 in the culture supernatant, 24-h conditioned medium was harvested with the addition of protease inhibitor mixture (Roche Applied Science). Medium was diluted 20-fold and subjected to Aβ40 ELISA analysis using a commercially available Aβ40 human ELISA kit (Invitrogen) according to the manufacturer's instructions. All experiments were performed at least three times independently.

Quantitative Real-time PCR—mRNA was isolated using RNeasy minikit from Qiagen following the manufacturer's instructions. A high capacity RNA-cDNA kit (Applied Biosystems, catalog no. 4387406) was used to make cDNA from RNA, following the manufacturer's instructions. Quantitative real-time PCR analysis was performed using the 7500 real-time PCR system (Applied Biosystems) using Taqman Fast universal PCR Master Mix (Applied Biosystems, catalog no. 4352042). Taqman gene expression assay probes used were Hs00234723_m1 (*SLC9A6* solute carrier family 9 (sodium/hydrogen exchanger), member 6), Hs00543518_m1 (*SLC9A9* solute carrier family 9 (sodium/hydrogen exchanger), member 9), and Hs00169098_m1 (*APP*). Hs02758991_g1 (*GAPDH*) was used as an endogenous control. *Ct* values were used for all manipulations and were first normalized to endogenous control levels by calculating the ΔCt for each sample. Values were then calculated relative to control to generate a $\Delta\Delta Ct$ value. -Fold change was calculated using the equation, expression -fold change $= 2^{-\Delta\Delta Ct}$. Each experiment was repeated three times independently.

Steady-state Transferrin Uptake—HEK 293 cells plated on polylysine-coated coverslips were rinsed and incubated in serum-free medium for 30 min to remove any residual transferrin and then were exposed to 100 μg/ml transferrin conjugated with Alexa Fluor 488 at 37 °C for 60 min. Uptake was stopped by chilling on ice and washing three times with ice-cold PBS. Bound transferrin was removed by an acid wash in PBS (pH 5.0), followed by a wash with PBS at pH 7.0. Cells were fixed with a solution of 4% paraformaldehyde, DAPI-stained, and mounted onto slides to determine colocalization of transferrin with NHE6-mCherry by confocal imaging.

Endosomal pH Measurement—Measurement of pH of transferrin-positive endosomal compartments was performed as described earlier. Briefly, HEK293 cells were rinsed and incubated in serum-free medium for 30 min to remove any residual transferrin and then were treated for 60 min with a pH-sensitive fluorescence indicator (Tfn-FITC) in conjunction with pH-insensitive cargo (Tfn-Alexa Fluor 633) (Molecular Probes) to normalize for endosomal loading. The fluorescence intensity of internalized transferrin was measured for ~10,000 cells by flow cytometry using the FACSAria instrument (BD Biosciences), and the average intensity of the cell population was recorded. For calibration of pH-dependent fluorescence, cells were exposed to K^+/H^+ ionophore nigericin (100 mM) and K^+-rich medium (125 mM KCl, 25 mM NaCl, 25 mM HEPES or 25 mM MES), adjusted to defined pH values (5.0, 6.0, 7.0, and 8.0).

Immunofluorescence and Image Quantification—Cultured cells on collagen-coated (SH-SY5Y) or polylysine-coated (HEK293) coverslips were preextracted with PHEM buffer containing 0.025% saponin for 2 min and then washed twice for 2 min with PHEM buffer containing 0.025% saponin and 8% sucrose. The cells were fixed with a solution of 4% paraformaldehyde (Electron Microscopy Sciences) and 8% sucrose in PBS for 30 min at room temperature. Cells were stained for primary antibodies and Alexa Fluor-conjugated secondary antibodies, DAPI-stained, and mounted onto slides using Dako fluorescent mounting medium. Cells were imaged using Zeiss AxioObserver inverted microscope with an LSM700 laser-scanning confocal module with advanced variable secondary dichroic beamsplitter that facilitates four-color imaging by eliminating fluorophore bleed-through. Slides were imaged with a ×63 oil immersion objective using four laser lines that excite at 405, 488, 561, and 639 nm. Expression of empty GFP vector and NHE6-GFP was detected using GFP (green) signal. Secondary antibodies without spectral overlap with DAPI and GFP fluorescence were selected. Alexa Fluor 568 (red) goat anti-mouse IgG (H + L) and Alexa Fluor 633 (far red) goat anti-rabbit IgG (H + L), both highly cross-adsorbed, were used for detecting subcellular markers and APP, respectively. The human eye is more sensitive to hues in the green and red color groups. Therefore, for better visualization of overlap between two images, we pseudocolored them green and red, and the colocalization was demonstrated by yellow fluorescence in the merge image. Fractional colocalization was determined from Manders' coefficient using the JACoP ImageJ plugin, which measures the direct overlap of green and red pixels in the confocal section and represents it as mean ± S.E. A minimum of 20 cells/condition from at least two representative experiments were included in the analysis.

Structural Modeling and Bioinformatics—Three-dimensional homology model structure of NHE6 was developed using the crystal structure of bacterial cation proton antiporter ortholog *Escherichia coli* NhaA as a template using multiple state-of-the-art approaches and evolutionary conservation analysis, as described earlier (1, 28). A brain RNA sequencing gene expression data set from 578 samples represented as log base 2 of RPKM (reads per kilobase of exon model per million mapped sequence reads) values across different developmental periods and different brain regions was obtained from the BrainSpan atlas (available on the World Wide Web). Hierarchical clustering with XLSTAT (Addinsoft, Paris, France) was performed under nearest neighbor methodology, and results were displayed as a dendrogram and heat map. Microarray data sets for the study included (*a*) GSE803 on the GPL8300 Affymetrix Human Genome U95 version 2 array analyzing gene expression in a variety of normal human tissues ($n = 24$) and (*b*) GSE1297 on the GPL96 Affymetrix Human Genome U133A array analyzing gene expression in different stages of AD (incipient, moderate, and severe) as compared with normal controls ($n = 31$). We validated our results by performing pooled analysis of gene expression profiles from independent studies of AD *versus* control brains, taken from anatomically and functionally distinct brain regions. To perform meta-analysis, we used normalized data obtained from Genevestigator (Nebion AG) that facil-

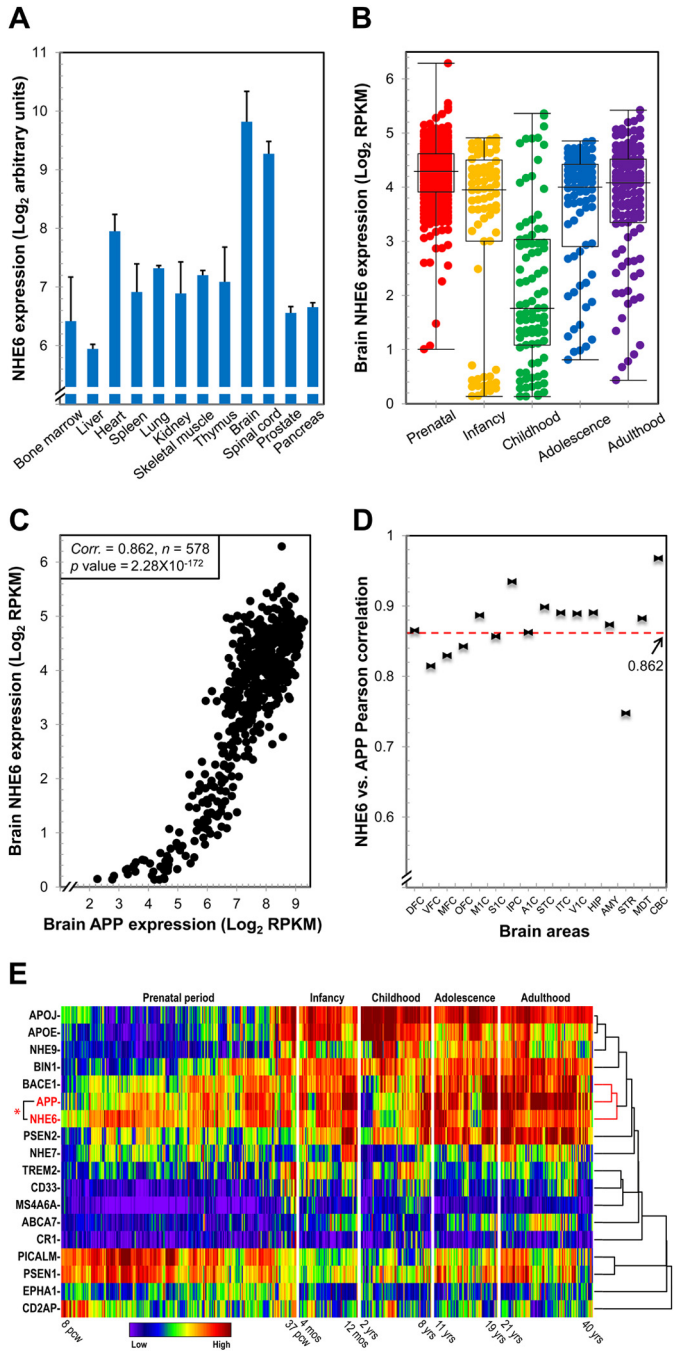

FIGURE 1. **Expression of NHE6 in brain is linked to APP.** *A*, NHE6 gene expression was extracted from the microarray data set of normal human tissues published by Yanai *et al.* (74). *B*, expression plots of NHE6 across different human development stages: prenatal period (embryogenesis to birth), infancy (birth to 1 year), childhood (2–10 years), adolescence (11–20 years), and adulthood (21 years and older). *C*, expression plot of NHE6 *versus* APP across a total of 578 samples obtained from different developmental periods. Note the prominent linear correlation of APP with NHE6 during normal human brain development (Pearson correlation coefficient, 0.86; $p = 2.28 \times 10^{-172}$). *D*, plot showing high Pearson correlation of NHE6 with APP expression across different brain regions. *Dashed red line*, average. *DFC*, dorsolateral prefrontal cortex (CTX) (Brodmann area 9 (BA9), BA46); *VFC*, ventrolateral prefrontal CTX (BA44, BA45); *MFC*, medial prefrontal CTX (BA32, BA33, BA34); *OFC*, orbital frontal CTX (BA11); *M1C*, primary motor CTX (BA4); *S1C*, primary somatosensory CTX (BA1–BA3); *IPC*, posterior inferior parietal CTX (BA40); A1C, primary auditory CTX (BA41); *STC*, posterior superior temporal CTX (BA22); *ITC*, inferior temporal CTX (BA20); *V1C*, primary visual CTX (BA17); *HIP*, hippocampal formation; *AMY*, amygdaloid complex; *STR*, striatum; *MDT*, mediodorsal nucleus of thalamus; *CBC*, cerebellar CTX. *E*, hierarchical clustering and expression heat map (from low (*blue*) to high (*red*)) of NHE6 with 15 genes strongly linked to Alzheimer disease showing clustering of NHE6 with early onset AD genes, including *APP* and *PSEN2*, and with the gene encoding β-secretase (*BACE1*). Notably, a strong association was observed for NHE6 with APP (*red asterisk*), similar to observations in *C*. The RNA sequencing gene expression data set included a total of 578 samples represented as log base 2 of reads per kilobase of exon model per million mapped sequence reads (*RPKM*) values across different developmental periods and different brain regions (data used for *B–E* were from the BrainSpan atlas Web site. *pcw*, post-conception weeks; *mos*, postnatal months; *yrs*, age in years. *Error bars*, S.D.

itates integration of data from multiple experiments. The pooled estimate and confidence interval of differential expression of NHE6, NHE7, and NHE9 genes were obtained using the RevMan program (Nordic Cochrane Centre). The I^2 statistic was used to assess heterogeneity among microarray data sets. An I^2 value more than 50% indicates the presence of significant heterogeneity (where more than 50% of the variation is due to heterogeneity rather than chance). A fixed effects model was used for data pooling for NHE7 ($I^2 = 14\%$) expression. For NHE6 ($I^2 = 65\%$) and NHE9 ($I^2 = 87\%$), a random effects (DerSimonian and Laird) model was used for data pooling due to observed substantial heterogeneity.

RESULTS

Expression of NHE6 in Brain Is Linked to APP—Although ubiquitous in tissue distribution, expression of NHE6 (*SLC9A6*) is highest in the spinal cord and brain (Fig. 1*A*), where it is particularly enriched in the hippocampus, cortex, and Purkinje cell layer of the cerebellum (1). Expression levels of NHE6 remain high through human development, including the adult (Fig. 1*B*). This distribution is consistent with emerging reports implicating NHE6 function in neurogenesis, spine dynamics, dendritic arborization, and synaptic strength (1, 17, 31). Similarly, impaired neurogenesis has been reported to occur early in AD pathology (32).

Genetic architecture and co-expression networks hold the key to understanding Alzheimer disease pathogenesis (33) and are based on the premise that genes that are expressed together are likely to function together (34). We noted that the pattern of APP expression closely parallels that of NHE6 through normal human brain development (Fig. 1*C*; Pearson correlation 0.86; $n = 578$; $p = 2.28 \times 10^{-172}$) and in all areas of the brain (*Fig. 1D*). In an independent analysis of the human brain RNA sequencing data, NHE6 was among the top 0.5% of human brain transcriptome transcripts (of 52,376) whose expression was most correlated with the expression of APP across 524 samples. In contrast, no correlation was observed between NHE6 and cytochrome c_1, an established housekeeping gene (29) (Pearson correlation 0.062; $n = 524$; $p = 0.15$). Next, we performed hierarchical clustering of brain NHE6 expression with 15 genes strongly linked to Alzheimer disease and found association of NHE6 with early onset AD genes, including *APP* and *PSEN2*, and with the gene encoding β-secretase (*BACE1*) (9, 11, 35) (Fig. 1*E*). Notably, clustering of NHE6 was distinct from that of related NHE isoforms (NHE9 and NHE7). We suggest that this clustering could provide clues to functional interactions and form the basis for new hypothesis-driven research, as evidenced by the close association of the enzyme-substrate pair (BACE1, APP) (10) and apolipoproteins (APOE, APOJ/

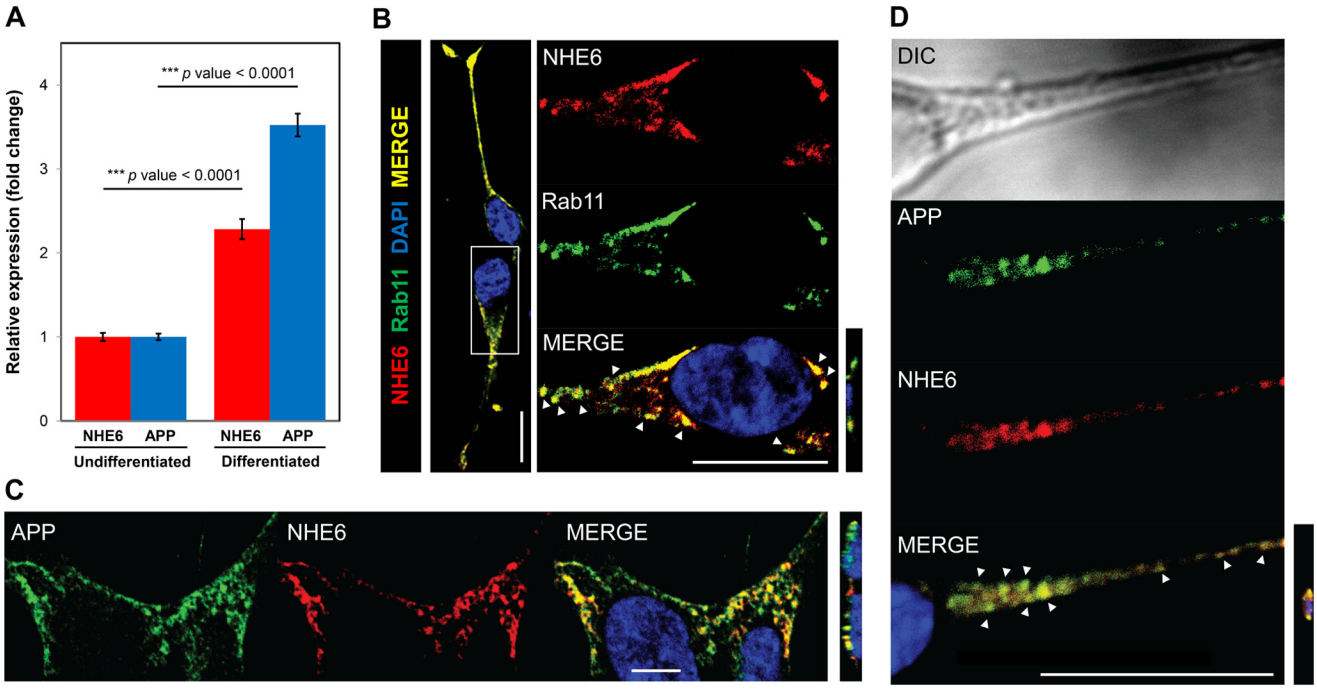

FIGURE 2. **NHE6 colocalizes with APP in differentiated SH-SY5Y cells.** *A*, quantitative PCR analysis of NHE6 and APP mRNA, in human SH-SY5Y neuroblastoma cells normalized to reference GAPDH. SH-SY5Y cells differentiated by sequential treatment with retinoic acid and brain-derived neurotrophic factor show a significant increase in APP and NHE6 expression. *Error bars*, S.D. determined from triplicate measurements. *B*, subcellular localization of endogenous NHE6 in differentiated SH-SY5Y cells determined by immunofluorescence confocal microscopy. The *merge image* (*left*) shows overlap of NHE6 (*red*) and recycling endosomal marker Rab11 (*green*). The *boxed region* is magnified for better representation (*right*). NHE6 (*red*) partly localizes with recycling endosome marker, Rab11 (*green*), as seen in the *merge*. An *orthogonal view* of subcellular localization is shown on the *extreme right* of the *merge image*. Colocalization of endogenous NHE6 (*red*) with APP (*green*) in undifferentiated SH-SY5Y cells (*C*) and differentiated neurites (*D*) is shown. *Orthogonal views* of subcellular localization are shown on the *extreme right* of the *merge images*. APP was immunostained using mouse monoclonal (6E10) antibody, and NHE6 was detected using rabbit polyclonal antibody raised against the C terminus. *Scale bars*, 10 μm. *DIC*, differential interference contrast.

clusterin) (36). Furthermore, recent studies have validated functional links between other close associations observed in our clustering analysis: *CD33* with *TREM2* (37) and *PICALM* with *PSEN1* (38). Intriguingly, we observed functional clustering of genes involved in innate immune responses implicated in AD (*TREM2*, *CD33*, and *MS4A6A*) (9, 35). These correlative observations prompted our hypothesis that ion transport activity and/or expression of NHE6 may contribute to AD pathology by altering luminal pH, endosomal trafficking, BACE1 activation, and Aβ production.

NHE6 Colocalizes with APP to Alter Trafficking in Cultured Cells—Human SH-SY5Y neuroblastoma cells can be differentiated with retinoic acid and brain-derived neurotrophic factor into cells with morphological and biochemical characteristics of mature neurons, which show increased expression of amyloid precursor protein (27, 39). We observed a ~3.5-fold increase in APP mRNA upon differentiation of SH-SY5Y cells that was accompanied by a significant increase in NHE6 expression (~2.3-fold) (Fig. 2*A*). Previously, we established that NHE6 localizes to endosomal recycling compartments and traffics in part to the plasma membrane (2). Using a rabbit polyclonal antibody raised against the C-terminal tail of NHE6, we localized endogenous NHE6 with recycling (Rab11) endosomal markers in SH-SY5Y cells (Fig. 2*B*), similar to previous observations in hippocampal neurons (17, 31). Colocalization of NHE6 with APP in both undifferentiated cells (Fig. 2*C*) and in differentiated neurites (Fig. 2*D*) was consistent with a potential role for NHE6 in APP function.

To further dissect the role of NHE6 in APP function, we utilized a well characterized HEK293-derived cell line stably expressing human APP695, developed by Choy *et al.* (40) for endosomal APP trafficking studies. Elegant studies by the Schekman group (40) using these cells have led to a model in which plasma membrane APP is endocytosed and trafficked to the *trans*-Golgi network (TGN), where the majority of processing occurs. Using an antibody that recognizes the C-terminal domain of human APP, as well as the β-CTF fragment, we show that APP colocalizes in part with the endosomal markers EEA1 and Rab11 and largely with the TGN marker Golgin 97, but not with the lysosomal marker lysobisphosphatidic acid (*LBPA*; Fig. 3*A*). As has been previously established, NHE6-GFP colocalized in part with the endosomal marker EEA1 and predominantly with transferrin-positive endosomes (not shown) (1, 2, 17). We noted prominent colocalization of APP with NHE6-GFP (Pearson correlation coefficient, 0.83 ± 0.03; Fig. 3*B*), similar to observations with endogenous NHE6 in differentiated SH-SY5Y cells (Fig. 2). Intriguingly, ectopic expression of NHE6-GFP resulted in striking redistribution of APP from the TGN to endosomes, resulting in increased colocalization with EEA1 and Rab11 (Fig. 3*C*), as quantified by Manders' coefficient (Fig. 3*D*). Redistribution of APP from the TGN also resulted in endocytic vesicles of variable sizes, similar to observations by Choy *et al.* (40). Given the emerging links between luminal pH and retrograde cargo exit out of endosomes (41), we hypothesized that the effect of elevated NHE6 activity on endosomal pH

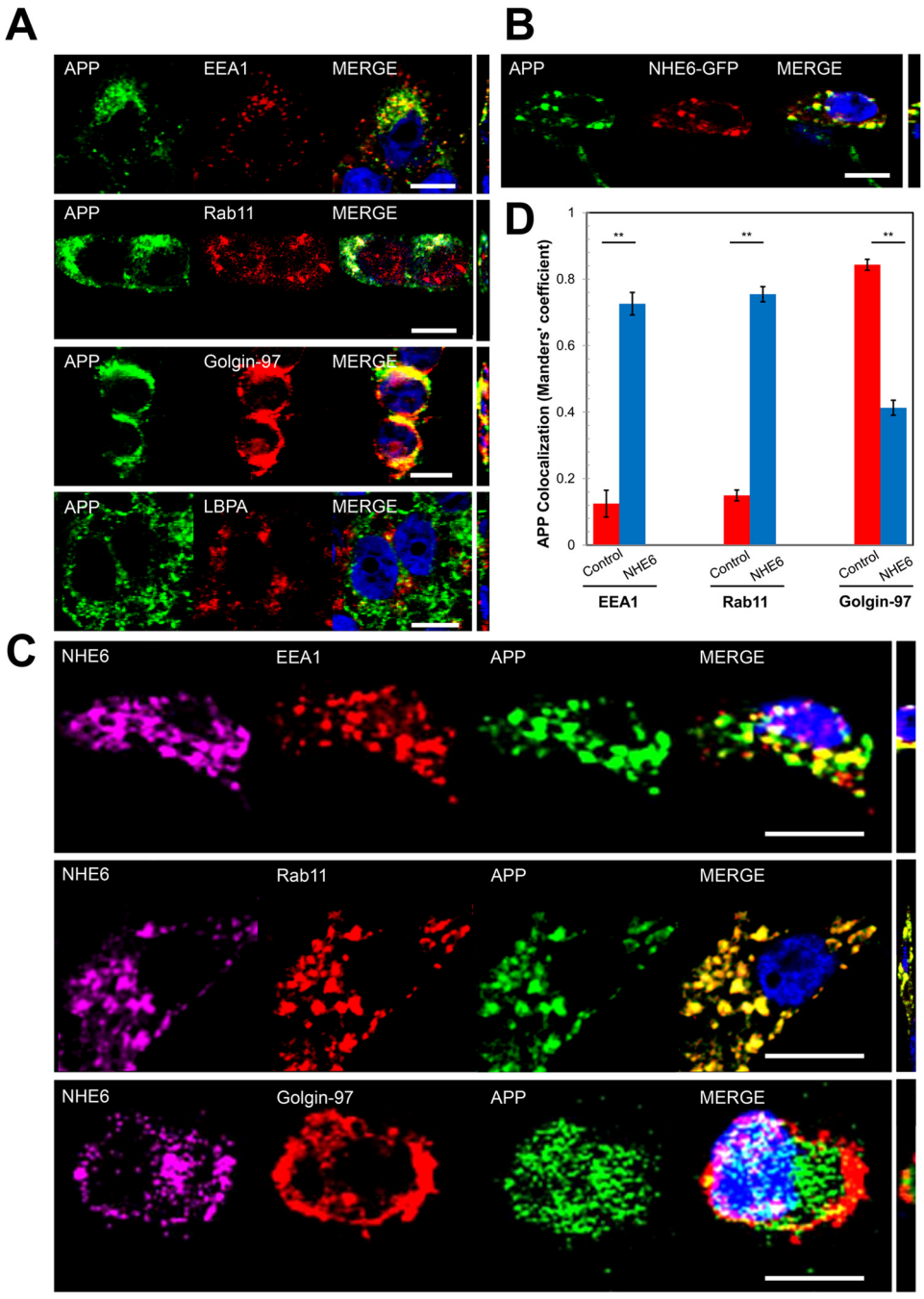

FIGURE 3. **NHE6 alters APP trafficking in HEK293-derived cells.** *A*, representative images of HEK293 cells stably expressing APP695 with empty vector transfection showing APP (in *green*) colocalization with different organelle markers indicated in *red*: EEA1 (early endosome), Rab11 (recycling endosome), Golgin 97 (*trans*-Golgi network), and lysobisphosphatidic acid (*LBPA*) (lysosome). Colocalization is indicated by *yellow* in the *merge* and in the *orthogonal view* (*extreme right*). *B*, representative image showing prominent colocalization (*yellow*) of APP (*green*) with NHE6-GFP (*red*). The Pearson correlation coefficient was 0.83 ± 0.03. *C*, NHE6 (*magenta*) coexpression alters localization of APP (*green*) from TGN to early/recycling endosomes. Organellar markers in *red* are as indicated. The *merged image* and *orthogonal view* (*extreme right*) in each *panel* show colocalization (in *yellow*) of APP with different organelle markers. *D*, quantification of steady-state APP localization with the indicated organellar markers in control cells (*red bars*) and with NHE6 coexpression (*blue bars*) using Manders' overlap coefficient (mean ± S.E. (*error bars*); $n = 20$; **, $p < 0.01$; two-tailed *t* test). *Scale bars*, 10 μm.

underlies the blockade of retrograde trafficking of APP from the endosome to the *trans*-Golgi network.

NHE6 and Monensin Alter APP Trafficking by Modulating Endosomal Acidification—The ionophore monensin mediates Na^+/H^+ exchange and mimics constitutively activated NHE6 to stimulate the endosomal recycling pathway and alter vesicular traffic (42, 43). Upon treatment of APP695-expressing HEK293 cells with monensin (1 μM for 8 h), APP redistributed from a perinuclear tubulo-reticular pattern into vesicles that colocalized prominently with the early endosomal marker EEA1, as quantified by Manders' coefficient (Fig. 4, *A*–*C*). This finding was strikingly analogous to the effect of NHE6 on APP trafficking and suggested that endosomal pH modulation was a common causal mechanism.

To measure endosomal pH, we took advantage of the overlap of NHE6 with endocytosed transferrin (Tfn), as shown in Fig.

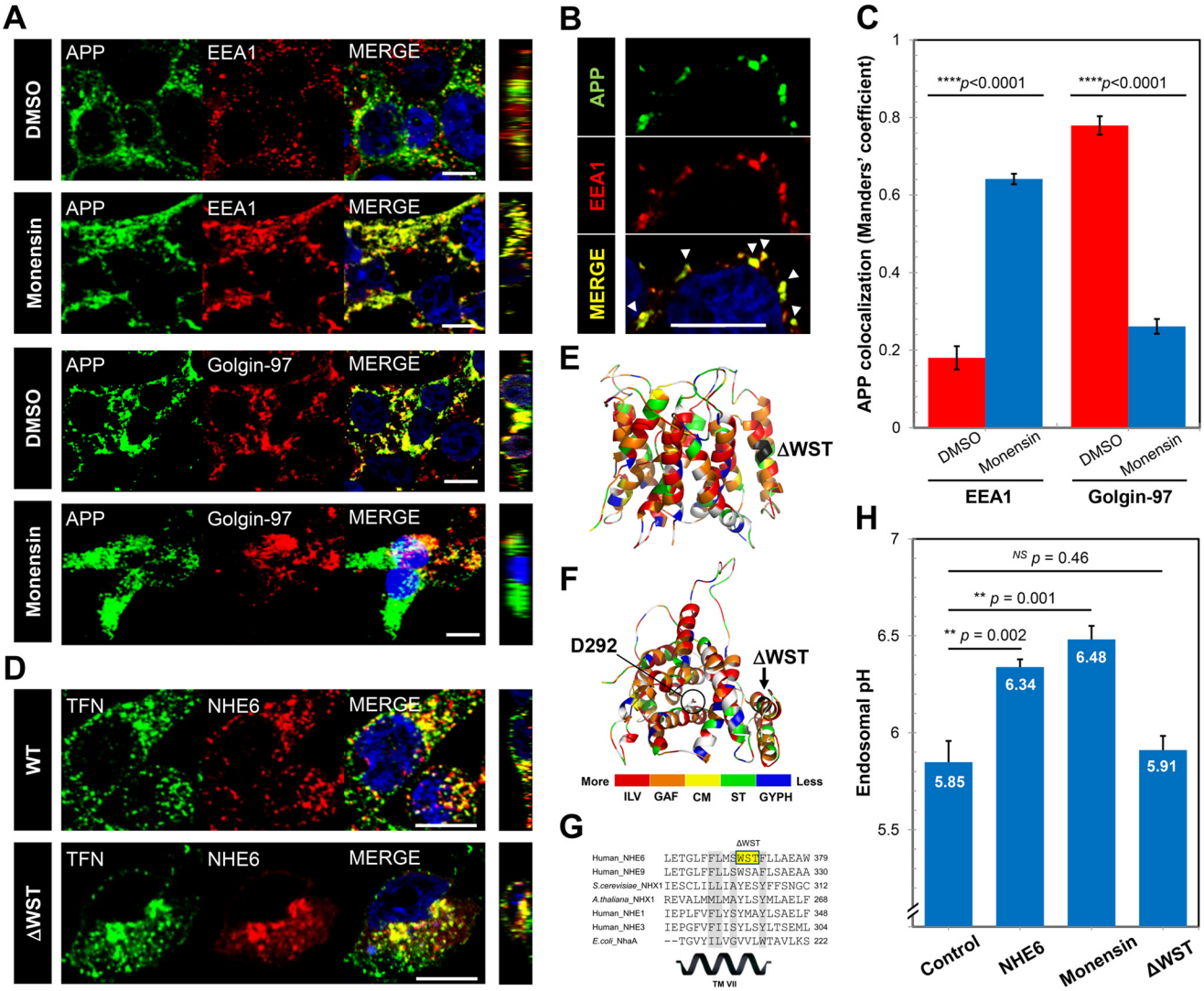

FIGURE 4. **Monensin mimics NHE6 in altering APP distribution and endosomal pH.** *A*, monensin treatment (1 μM for 8 h) alters localization of APP from TGN to endosomes. Shown are representative images of HEK293 cells stably expressing APP695 with control (DMSO) or monensin treatment showing localization of APP (*green*) with organellar markers in *red* (EEA1, early endosome; Golgin 97, *trans*-Golgi network). Colocalization is indicated by *yellow* in the *merge* and in the *orthogonal view* (*extreme right*). *B*, representative magnified image of monensin-treated cells showing prominent overlap of APP (*green*) with endosomal marker EEA1 (*red*). *C*, quantification of steady-state APP localization with the indicated organellar markers in control cells (*red bars*) and with monensin treatment (*blue bars*) using Manders' overlap coefficient (mean ± S.E.; $n = 20$; ****, $p < 0.0001$; two-tailed *t* test). *D*, localization of mCherry-tagged NHE6 and ΔWST^{372} patient mutant to transferrin-positive endosomes in HEK293 cells. NHE6 and the mutant (both in *red*) colocalize with Alexa Fluor-tagged transferrin after 1 h of uptake (*green*), as described under "Experimental Procedures." Shown are *side* (*E*) and *cytoplasmic* (*F*) *views* of a model structure of the transporter domain of NHE6 based on the structure of *E. coli* NhaA and *colored* according to the hydrophobicity scale adopted by Kojetin *et al.* (75), with the *color bar* at the *bottom*. The position of ΔWST^{372} mutant is shown in *black*. Note that amino acids facing the lipid bilayer are mostly hydrophobic, as expected. The putative proton-binding Asp-292 residue important for transport function is shown by a *stick representation*. *G*, alignment of human NHE6, NHE9, NHE1, and NHE3 sequences with *S. cerevisiae* Nhx1, *Arabidopsis thaliana* Nhx1, and *E. coli* NhaA was performed using evolutionary conservation analysis, and the patient mutation was localized to a region corresponding to transmembrane helix VII in NhaA. *H*, monensin and expression of wild type but not mutant NHE6 alkalinizes endosomal lumen. pH of transferrin-positive endosomes in HEK293 cells was determined in (*a*) control, (*b*) cells with NHE6 overexpression, (*c*) cells expressing ΔWST^{372} disease-associated mutation in NHE6, and (*d*) cells treated with monensin. A pH-sensitive fluorescence indicator (Tfn-FITC) was used in conjunction with pH-insensitive cargo (Tfn-Alexa Fluor 633) to measure endosomal pH. Monensin treatment and expression of NHE6, but not the disease-associated ΔWST^{372} mutation, resulted in significant alkalization of endosomal pH (mean ± S.D.; *NS*, not significant; $n = 3$; **, $p < 0.01$; two-tailed *t* test). *Scale bar*, 10 μm.

4*D*. We measured endosomal pH by a ratiometric method using Tfn coupled to a mixture of pH-sensitive (Tfn-FITC) and pH-insensitive (Tfn-Alexa Fluor 633) fluorescence probes to normalize for endosomal loading, as described under "Experimental Procedures." We expressed NHE6 with a C-terminal mCherry tag to avoid spectral overlap with FITC-tagged transferrin. NHE6 expression alkalinized endosomal pH from 5.85 ± 0.11 to 6.34 ± 0.04 (Fig. 4*H*). These results are consistent with endosomal alkalization observed by Xinhan *et al.* (44) in HeLa overexpressing NHE6 and hyperacidification seen in NHE6-knockdown cells. Luminal endosomal pH in HEK293 cells treated with monensin was also elevated (to 6.48 ± 0.07), similar to cells expressing NHE6-mCherry (Fig. 4*H*).

To rule out nonspecific overexpression effects, we examined a patient-associated mutation within the membrane-embedded transporter domain of NHE6, which was predicted to result in loss of function (1). Specifically, ΔWST^{372} is an in-frame deletion of three amino acids that was described by Garbern *et*

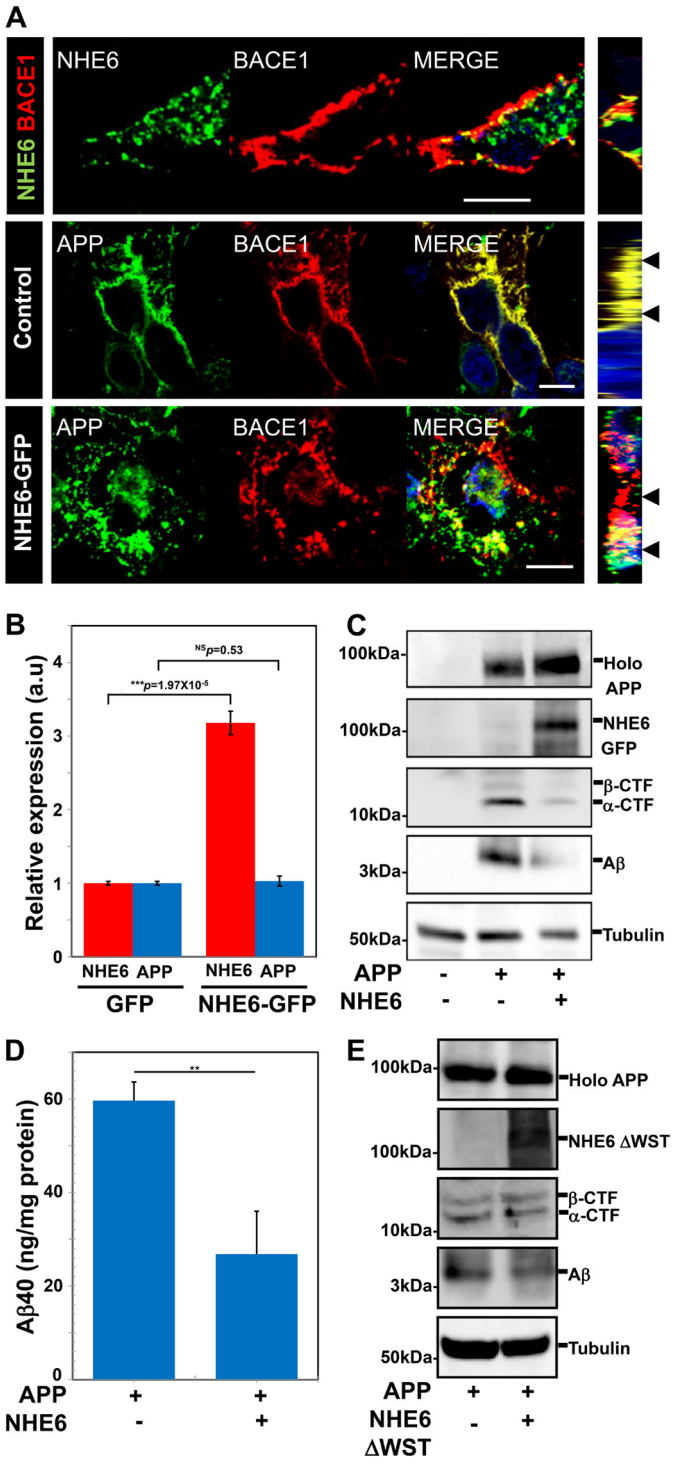

FIGURE 5. **NHE6 alters APP processing in cultured cells.** *A* (*top*), representative image showing less colocalization (*yellow*) of BACE1 (*red*) with NHE6-GFP (*green*) in HEK293 cells. Colocalization is indicated by *yellow* in the *merge* and in the *orthogonal view* (*extreme right*). *Middle*, representative image of HEK293 cells stably expressing APP695 with empty vector (control) and BACE1 transfection showing prominent colocalization of APP (*green*) with BACE1 (*red*). *Bottom*, cotransfection of NHE6-GFP and BACE1 into APP stable cells shows vesicular redistribution of APP (*green*) and reduced overlap of APP with BACE1 (*red*). Note the prominent APP-BACE1 colocalization in control cells and less colocalization in cells with elevated levels of NHE6 in the orthogonal view of the *merge* (*black arrows*). *B*, quantitative PCR analysis showing the efficacy of overexpression of NHE6-GFP in HEK293 stably expressing APP695. The data are plotted as average -fold change of mRNA levels relative to control levels, with S.D. (*error bars*) determined from triplicate measurements. *C*, Western blot analysis showed significant reduction in Aβ levels with NHE6 coexpression and concomitant increase in full-length APP. Note reductions in both α-CTF and β-CTF forms suggesting a perturbation in trafficking/activity of multiple secretase enzymes. NHE6-GFP was detected using anti-GFP antibody. *D*, quantitation of Aβ40 by ELISA showed a significant reduction of secreted Aβ peptide from cells expressing elevated levels of NHE6 (mean ± S.D.; **, $p < 0.01$; $n = 3$; two-tailed *t* test). Total Aβ in the conditioned medium was normalized to total cellular protein. *E*, expression of disease-associated ΔWST^{372} loss-of-function mutant in HEK293 cells stably expressing APP695 fails to significantly alter APP processing. Western blot analysis was performed with lysates collected from control cells with mCherry empty vector and cells transfected with NHE6ΔWST^{372}-mCherry (detected using anti-mCherry rat monoclonal antibody). Holo-APP was detected using polyclonal C-terminal antibody, and tubulin was used as a loading control.

al. (18) in patients with severe intellectual disability and autistic symptoms accompanied by neuronal loss and Tau deposition in the brain. For a structure-driven assessment of NHE6 variants, we developed a three-dimensional model structure of NHE6 on the basis of the inward-open NhaA crystal structure using evolutionary conservation-based approaches, described previously (1, 28). We mapped the ΔWST^{372} mutation within the membrane-embedded transporter domain that corresponds to transmembrane helix VII in NhaA, predicted to be non-functional (Fig. 4, *E–G*). Quantitative PCR showed ~80% expression of the mutant transcript relative to wild-type NHE6. We confirmed that cell viability, measured by trypan blue exclusion, remained unaltered by manipulations in NHE6 (vector control, 95.70 ± 1.23%; NHE6 expression, 94.45 ± 1.57%; ΔWST^{372} expression, 95.75 ± 1.54%; percentages represent the proportion of viable unstained cells relative to the total cells counted). NHE6 carrying the ΔWST^{372} mutation colocalized with transferrin (Fig. 4*D*) but failed to elevate endosomal pH in HEK293 cells (Fig. 4*H*), confirming loss of function as predicted using a structure-function approach. Taken together, these results establish perturbations in endosomal pH as an important causal mechanism in subcellular APP redistribution.

NHE6 Alters APP Processing in Cultured Cells—Several lines of evidence suggest that BACE1 is predominantly localized to the *trans*-Golgi network, where the majority of APP processing occurs (30, 40). We hypothesized that as an evolutionarily conserved mechanism for protection against excess endosomal acidification, NHE6 activity might be one of the fundamental strategies by which neurons largely restrict APP and BACE1 to separate organelles, thus limiting generation of Aβ under normal physiological conditions. To test this hypothesis in our cell culture model, we transfected the BACE1 construct into HEK293-derived cells stably expressing APP695 and confirmed prominent colocalization of APP with BACE1 (Pearson correlation coefficient, 0.89 ± 0.04; Manders' overlap coefficient, 0.83 ± 0.05; $n = 30$; Fig. 5*A*), as reported in the literature (30). Intriguingly, unlike APP (Fig. 3*B*), BACE1 did not show much colocalization with NHE6-GFP in HEK293 cells (Pearson correlation coefficient, 0.39 ± 0.08; Manders' overlap coefficient, 0.22 ± 0.06; $n = 20$; Fig. 5*A*). Upon cotransfection of NHE6-GFP and BACE1 into APP stable cells, we documented prominent colocalization of APP with NHE6-GFP and reduced overlap of APP with BACE1. Quantitative analysis using Manders' coefficient revealed the fraction of APP overlapping with BACE1 to

decrease from 0.83 ± 0.05 to 0.39 ± 0.11 ($p = 8.27 \times 10^{-28}$; $n = 30$) upon NHE6-GFP expression. In previous studies, treatment of cells stably expressing APP with destruxin E, a V-ATPase inhibitor, resulted in a similar decrease in colocalization of APP with BACE1 and reduced processing of APP and Aβ generation (45). Inhibition of V-ATPase is expected to alkalinize endosomes and mimic the activity of NHE6, consistent with a critical role for endosomal pH in Aβ biogenesis.

Upon NHE6-GFP lentivirus-mediated expression in stable APP695 cells, quantitative PCR analysis showed that expression of NHE6 mRNA was enhanced by 3.2-fold ($p = 1.97 \times 10^{-5}$; two-tailed *t* test), whereas APP mRNA levels remained unaltered ($p = 0.53$; two-tailed *t* test (Fig. 5*B*). Choy *et al.* (40) have reported that depletion of retromer subunits interrupts retrograde trafficking of APP from the endosomes to TGN and reduces Aβ production in the stable APP695 cell culture model. Considering that NHE6 overexpression also blocked delivery of APP to TGN, we predicted a similar effect. NHE6 is known to regulate clathrin-dependent endocytosis and modulate endosomal pH (44); therefore, we hypothesized that NHE6 activity could potentially alter (*a*) α-site cleavage of cell surface APP by endocytosis via clathrin-coated pits and (*b*) β-site cleavage of APP by modulation of luminal pH and β-secretase activity. Consistent with our hypothesis, Western blot analysis showed that ectopic expression of NHE6-GFP in HEK293 cells stably expressing APP695 significantly reduced Aβ levels and concomitantly increased full-length APP (Fig. 5*C*). We also noted reductions in both CTF forms, suggesting a perturbation in trafficking and/or activity of multiple secretase enzymes. HEK293 cells stably expressing APP695 produce low levels of Aβ42 (40); hence, we did not measure secreted Aβ42. Quantitation by ELISA (Fig. 5*D*) confirmed a significant reduction of secreted Aβ40 peptide from cells expressing elevated levels of NHE6. We also confirmed that expression of ΔWST^{372} loss-of-function NHE6 mutant failed to significantly alter APP processing (Fig. 5*E*). Intriguingly, our findings with NHE6 recapitulate multiple studies in the literature, conducted over the past 2 decades reporting the effects of monensin on APP processing (46–49). Like NHE6, monensin has been shown to increase full-length APP expression, enhance intracellular accumulation of APP, inhibit β-secretase activity, and alter APP processing (46–49). Therefore, our new findings present a physiological and mechanistic basis for beneficial effects of monensin and strengthen the validity of endosomal pH as a therapeutic target for Alzheimer disease.

We next investigated whether NHE6 knockdown altered the processing of amyloid precursor protein. Lentivirus-mediated knockdown of NHE6 (by ~70%; *p* value = 3.07×10^{-05}; two-tailed *t* test; Fig. 6*A*) in HEK293 cells stably expressing APP did not alter transcript levels for APP. We consistently observed a compensatory increase in NHE9 levels (by ~3-fold; *p* value = 0.014; two-tailed *t* test) upon knockdown of NHE6, similar to our previous observations in primary astrocytes (28). Quantitation of Western blot signal intensity analysis showed ~80% depletion (*p* value = 0.015; two-tailed *t* test) of NHE6 protein by lentiviral knockdown (Fig. 6, *B* and *C*). We confirmed that cell viability, measured by trypan blue exclusion, remained unal-

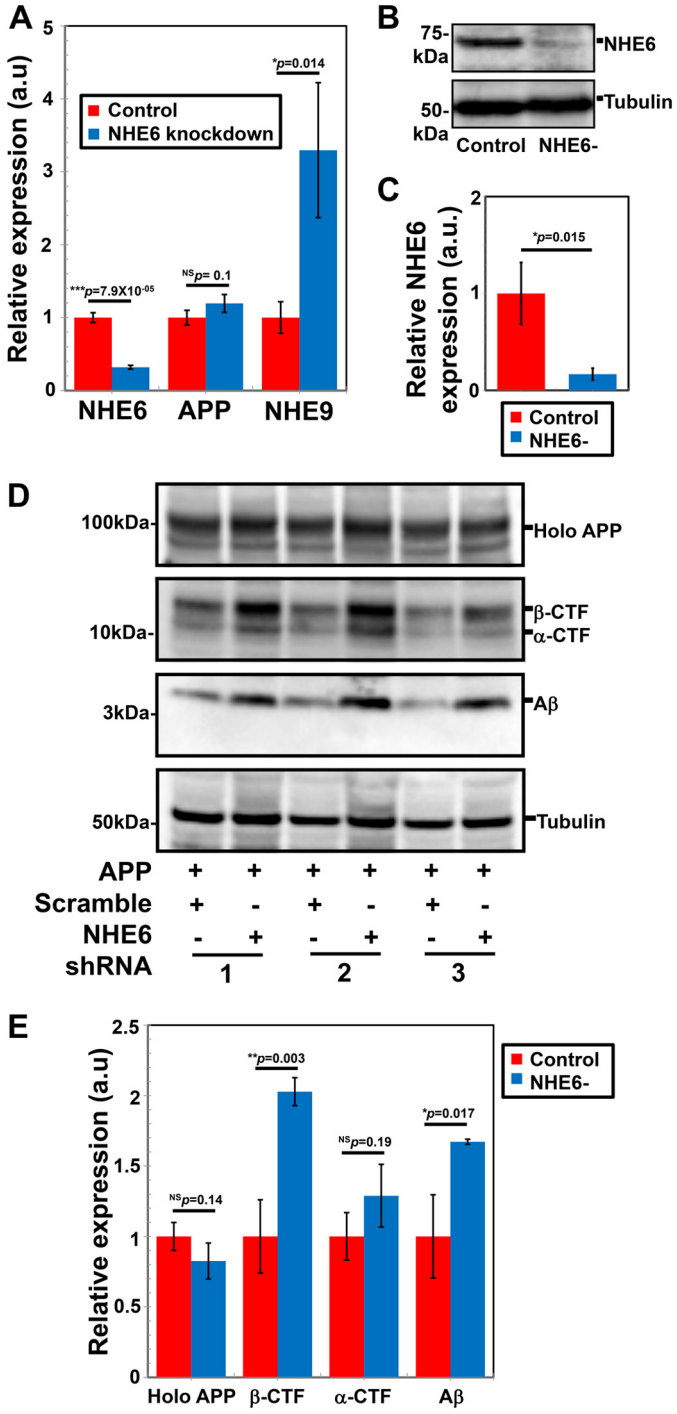

FIGURE 6. **NHE6 depletion enhances amyloidogenic processing of APP.** *A*, quantitative PCR analysis showing the efficacy of short hairpin RNA knockdown of NHE6 in HEK293 cells stably expressing APP695. The data are plotted as average -fold change of mRNA levels relative to control levels, with S.D. (*error bars*) determined from triplicate measurements. Note the compensatory increase in NHE9 levels upon knockdown of NHE6, similar to previous observations in primary astrocytes (28). Shown are a representative Western blot (*B*) and quantification of three biological replicates (*C*) showing the efficacy of short hairpin RNA knockdown of NHE6 (*NHE6*−) normalized to tubulin levels. Control cells were transfected with scrambled shRNA, and NHE6 was detected using rabbit polyclonal antibody raised against the C terminus. Western blot analysis (*D*) and densitometry quantification (*E*) of three biological replicates demonstrated a significant increase in β-CTF and Aβ levels with NHE6 depletion. Holo-APP was detected using monoclonal 6E10 antibody, and tubulin was used as a loading control. *a.u.*, arbitrary units.

TABLE 1

Reduced NHE6 transcript expression in Alzheimer disease brains

Differential NHE6, NHE7, and NHE9 expression between AD and control (Ctrl) data sets and pooled average represented as mean difference and 95% confidence interval (CI) of log base 2 expression, as depicted in Fig. 7, *B–D*, were obtained as described under "Experimental Procedures." The publicly available microarray data sets are from anatomically and functionally distinct brain regions taken from three independent studies (51–53) comprising a total of 96 AD and 82 control post-mortem brains. Pooled analysis from weighted data sets (indicated in columns) showed significant down-regulation of NHE6 in AD brains. In contrast, pooled analysis of expression of related intracellular Na^+/H^+ exchangers, NHE7 and NHE9, did not show significant difference between AD and control groups. *NS*, not significant; *, $p < 0.05$; **, $p < 0.01$; ***, $p < 0.00001$.

Data set	Brain area	Sample size AD	Sample size Ctrl	NHE6 Differential expression, 95% CI	NHE6 Weight	NHE7 Differential expression, 95% CI	NHE7 Weight	NHE9 Differential expression, 95% CI	NHE9 Weight
				log_2 arbitrary units	*%*	*log_2 arbitrary units*	*%*	*log_2 arbitrary units*	*%*
1	Superior temporal gyrus (52)	22	9	-1.27 (-1.75, -0.79)***	15.6%	0.06 (-0.13, 0.25)^{NS}	13.0%	-0.07 (-0.29, 0.15)^{NS}	12.30%
2	Parietal lobe (53)	4	4	-0.12 (-1.16, 0.92)^{NS}	8.8%	-0.07 (-0.22, 0.07)^{NS}	22.6%	-0.41 (-0.55, -0.27)***	13.60%
3	Primary visual cortex (52)	17	12	-0.84 (-1.62, -0.06)*	11.6%	0.05 (-0.10, 0.20)^{NS}	20.0%	0.11 (-0.09, 0.31)^{NS}	12.60%
4	Middle temporal gyrus (52)	15	12	-2.05 (-2.75, -1.35)***	12.7%	-0.25 (-0.47, -0.04)*	9.6%	-0.07 (-0.23, 0.10)^{NS}	13.20%
5	Entorhinal cortex (52)	10	12	-1.17 (-2.03, -0.31)**	10.7%	-0.05 (-0.22, 0.12)^{NS}	16.0%	0.31 (-0.01, 0.64)^{NS}	10.30%
6	Entorhinal cortex (51)	9	8	-0.29 (-0.96, 0.38)^{NS}	13.1%	0.09 (-0.23, 0.41)^{NS}	4.5%	-0.05 (-0.27, 0.17)^{NS}	12.30%
7	Posterior cingulate cortex (52)	9	13	-1.53 (-2.20, -0.86)***	13.0%	0.11 (-0.15, 0.37)^{NS}	6.7%	0.18 (-0.04, 0.40)^{NS}	12.30%
8	Hippocampus (52)	10	12	-1.53 (-2.08, -0.98)***	14.7%	-0.08 (-0.32, 0.17)^{NS}	7.6%	0.30 (0.15, 0.45)**	13.40%
Pooled effect		**96**	**82**	**-1.15 (-1.56, -0.74)*****	**100%**	**-0.03 (-0.09, 0.04)^{NS}**	**100%**	**0.03 (-0.16, 0.22)^{NS}**	**100%**

TABLE 2

NHE6 correlates with synapse genes down-regulated in AD

Pearson correlation coefficient of hippocampal expression of NHE6 with 22 different synapse genes down-regulated in AD and 20 synapse genes up-regulated in AD in microarray data reported by Blalock *et al.* (50, 57). Correlations of NHE6 with synapse genes were calculated across all 31 subjects, including control and clinical stages of AD. Note the positive correlation of NHE6 with most genes down-regulated in AD and negative NHE6 correlation with most genes up-regulated in AD, suggesting that changes in synapse genes in AD involve a cellular mechanism that includes NHE6.

Down-regulated genes			Up-regulated genes		
Gene	Pearson correlation with NHE6	*p* value	Gene	Pearson correlation with NHE6	*p* value
NRXN1	0.92	9.74×10^{-14}	*CHRNB3*	-0.71	5.94×10^{-6}
GABBR2	0.90	1.59×10^{-12}	*CTBP2*	-0.64	8.78×10^{-5}
SV2B	0.86	2.73×10^{-10}	*USH1C*	-0.59	4.20×10^{-4}
ITPR1	0.83	4.88×10^{-9}	*CASK*	-0.58	6.10×10^{-4}
NEFM	0.83	5.72×10^{-9}	*GRIK3*	-0.52	2.60×10^{-3}
GRIA2	0.71	6.34×10^{-6}	*GLRA3*	-0.49	4.79×10^{-3}
C2CD5	0.66	3.95×10^{-5}	*GABRQ*	-0.44	0.01
PSD3	0.63	1.47×10^{-4}	*SYNC1*	-0.40	0.02
FAIM2	0.55	1.17×10^{-3}	*DLG1*	-0.39	0.03
CADPS2	0.54	1.74×10^{-3}	*SSPN*	-0.31	0.09
DMD	0.53	2.06×10^{-3}	*CHRNA9*	-0.30	0.10
PPT1	0.53	2.12×10^{-3}	*PPP1CC*	-0.24	0.19
RIMS2	0.51	2.92×10^{-3}	*HOMER3*	-0.24	0.19
ELOVL2	0.48	5.79×10^{-3}	*ITGB1*	-0.08	0.66
RAB3B	0.47	6.77×10^{-3}	*CHRNA1*	0.00	0.99
CABP1	0.46	8.73×10^{-3}	*SNPH*	0.33	0.07
SHANK2	0.42	1.75×10^{-2}	*ICA1*	0.35	0.05
LZTS1	0.22	0.22	*DLGAP2*	0.40	0.03
MCTP1	0.14	0.46	*GABRA5*	0.63	1.15×10^{-4}
COLQ	0.13	0.49	*CDK5R1*	0.79	1.12×10^{-7}
NUFIP1	-0.19	0.29			
NRG1	-0.23	0.20			

tered by NHE6 knockdown (scrambled control, 95.40 ± 1.12%; NHE6 knockdown, 96.45 ± 1.63%; percentages represent the proportion of viable unstained cells relative to the total cells counted). Although overlapping distribution of the closely related NHE9 paralog could result in functional redundancy and thus underestimate functional effect in cultured cell models, Western blot analysis showed a significant increase in levels of β-CTF (2.03-fold; p value = 0.003; two-tailed t test) and Aβ levels (1.67-fold; p value = 0.017; two-tailed t test) upon NHE6 knockdown (Fig. 6, *D* and *E*). We also observed a reduction in full-length APP (by 17.4%) and increase in α-CTF (1.29-fold), although the differences did not reach statistical significance. Notably, NHE6 depletion has been previously shown to cause hyperacidification of endosomes both in cell culture models and in primary neurons (17, 44). Taken together, these findings indicate that NHE6 functions as a proton leak pathway in endosomes acting as a brake against excessive amyloidogenic processing of APP by controlling luminal acidification.

Reduced NHE6 Expression in Alzheimer Disease Brains—We investigated whether the expression of NHE6 was altered in AD brains by analyzing publically available microarray data, as described under "Experimental Procedures." We found statistically significant reduction of NHE6 gene expression in different stages of AD (incipient, moderate, and severe), as compared with normal controls, in microarray data reported by Blalock *et al.* (50) (n = 31; $p < 0.05$; ANOVA); Fig. 7*A*). Furthermore, independent studies of gene expression profiles from anatomically and functionally distinct brain regions showed that NHE6 was down-regulated in AD brains, with a pooled average of -1.15 ($p < 0.00001$; Fig. 7*B* and Table 1) (51–53). In contrast, pooled analysis of NHE7 and NHE9 expression did not show a

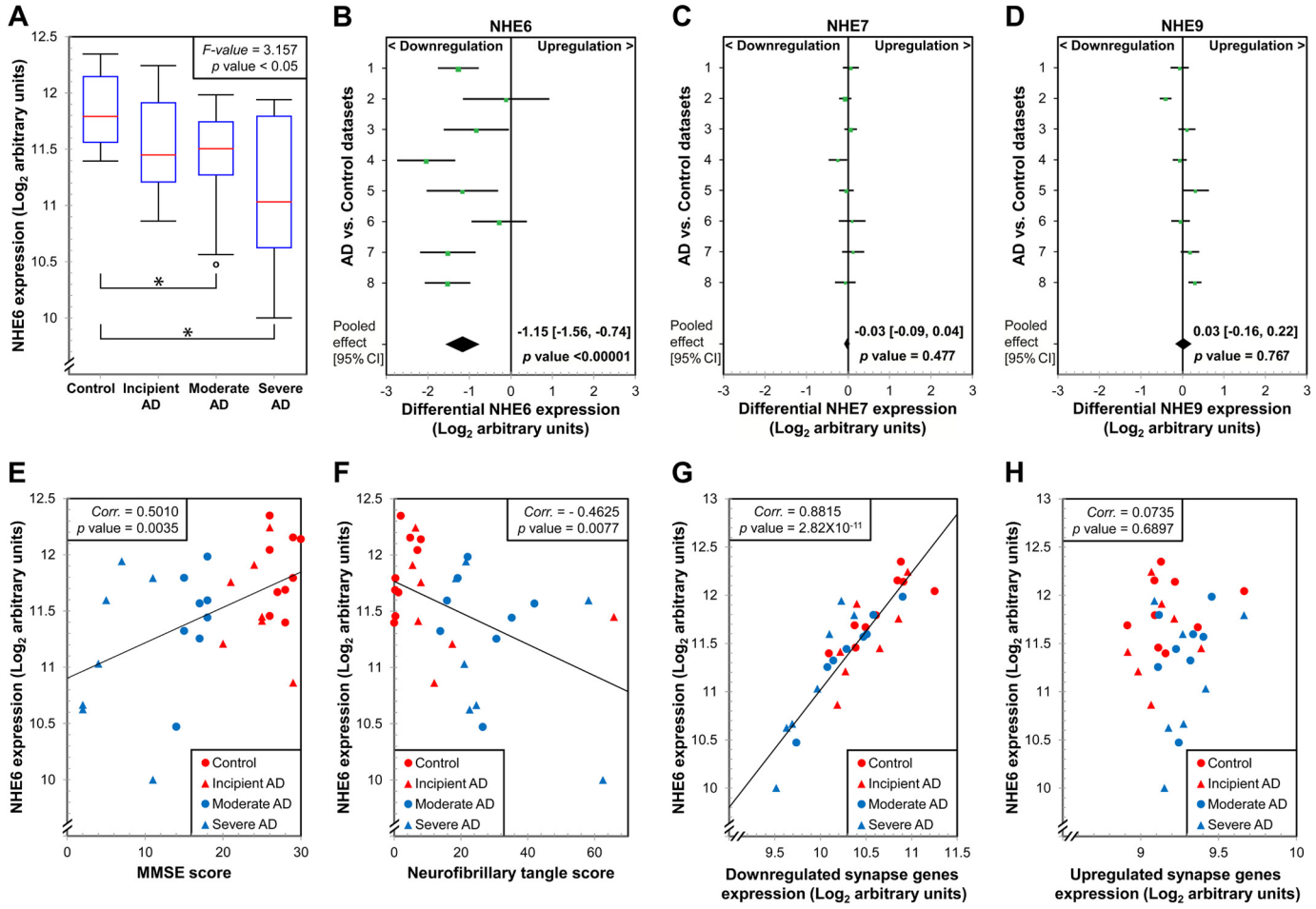

FIGURE 7. **Reduced NHE6 transcript box and whisker in Alzheimer disease brains.** *A*, box and whisker plots of hippocampal NHE6 gene expression across control and clinical stages of AD in microarray data reported by Blalock *et al.* (50) ($n = 31$; *, $p < 0.05$; ANOVA). *B*, differential NHE6 expression between AD and control from data described in Table 1, represented as a Forest plot of mean difference and 95% confidence interval (*CI*) of log base 2 expression. *Black diamond*, pooled average of −1.15 (95% CI: −1.56, −0.74) (*Z*-test, 5.47; control, $n = 82$; AD patients, $n = 96$; $p < 0.00001$). *C*, differential NHE7 expression between AD and control from data described in Table 1, represented as a Forest plot of mean difference and 95% confidence interval of log base 2 expression. *Black diamond*, pooled average of −0.03 (−0.09, 0.04) (*Z*-test, 0.72; control, $n = 82$; AD patients, $n = 96$; $p = 0.47$). *D*, differential NHE9 expression between AD and control from data described in Table 1, represented as a Forest plot of mean difference and 95% confidence interval of log base 2 expression. *Black diamond*, pooled average of 0.03 (−0.16, 0.22) (*Z*-test, 0.30; control, $n = 82$; AD patients, $n = 96$; $p = 0.76$). *E*, expression plot of NHE6 with ante-mortem cognitive function evaluated by MMSE scores across all 31 subjects, from data reported by Blalock *et al.* (50). Scores on the MMSE range from 0 to 30, with scores of 27 or higher indicating normal cognitive function. Reductions in NHE6 levels were associated with poor MMSE scores (Pearson correlation coefficient, 0.50; $n = 31$; $p = 0.0035$). *F*, expression plot of NHE6 with post-mortem brain Tau pathology assessed via neurofibrillary tangle scores across all 31 subjects, regardless of diagnosis. Higher neurofibrillary tangle scores indicate worse neuropathology and were associated with reduced NHE6 expression (Pearson correlation coefficient, −0.46; $n = 31$; $p = 0.0077$). Linear fit (*black line*) shown in *E* and *F* depicts positive and negative correlations, respectively. *G*, expression plot of NHE6 *versus* APP with average log base 2 expression of 22 synapse-associated genes found down-regulated in AD across all 31 subjects in the data set of Blalock *et al.* (50, 57). NHE6 levels strongly correlated with the synapse genes (Pearson correlation coefficient, 0.88; $n = 31$; $p = 2.82 \times 10^{-11}$), suggesting that changes in synapse genes in AD, at least in part, involve a cellular mechanism that includes NHE6. *H*, expression plot of NHE6 *versus* APP with average log base 2 expression of 20 synapse-associated genes found up-regulated in AD showed a lack of correlation (Pearson correlation coefficient, 0.07; $n = 31$; $p = 0.6897$). *Error bars* in *B–D* are the 95% confidence interval of differential expression.

significant difference between AD and control groups (Fig. 7, *C* and *D*). To evaluate the clinico-pathological correlation of NHE6 expression with AD phenotypes, we tested the association of NHE6 gene expression with ante-mortem cognitive function evaluated by means of the mini-mental state examination (MMSE; positive correlation, $p = 0.0035$; Fig. 7*E*) and with post-mortem brain Tau pathology assessed via neurofibrillary tangle scores (negative correlation, $p = 0.0077$; Fig. 7*F*). These correlations suggest that reduced NHE6 expression and, by extrapolation, reduced endosomal pH may underlie AD phenotypes. We then hypothesized that changes in NHE6 are associated with broader changes in gene expression, such as down-regulation of synapse genes, known to occur in AD (54, 55). Notably, synaptic loss occurs early in pathogenesis of AD and precedes neuronal loss by several decades (56). To investigate our hypothesis, we evaluated Pearson correlation of NHE6 levels with average expression of 22 synapse-associated genes found to be down-regulated in AD in the data set of Blalock *et al.* (50, 57). As shown in Fig. 7*G*, NHE6 levels strongly correlated with the synapse genes (Pearson correlation coefficient, 0.88; $p = 2.82 \times 10^{-11}$), suggesting that changes in synapse genes in AD, at least in part, involve a cellular mechanism that includes NHE6. Notably (Table 2), NHE6 showed a strong association with neurexin-1 (*NRXN1*; Pearson correlation coefficient, 0.92), GABA-B receptor 2 (*GABBR2*; Pearson correlation coefficient, 0.90), and synaptic vesicle glycoprotein 2B (*SV2B*;

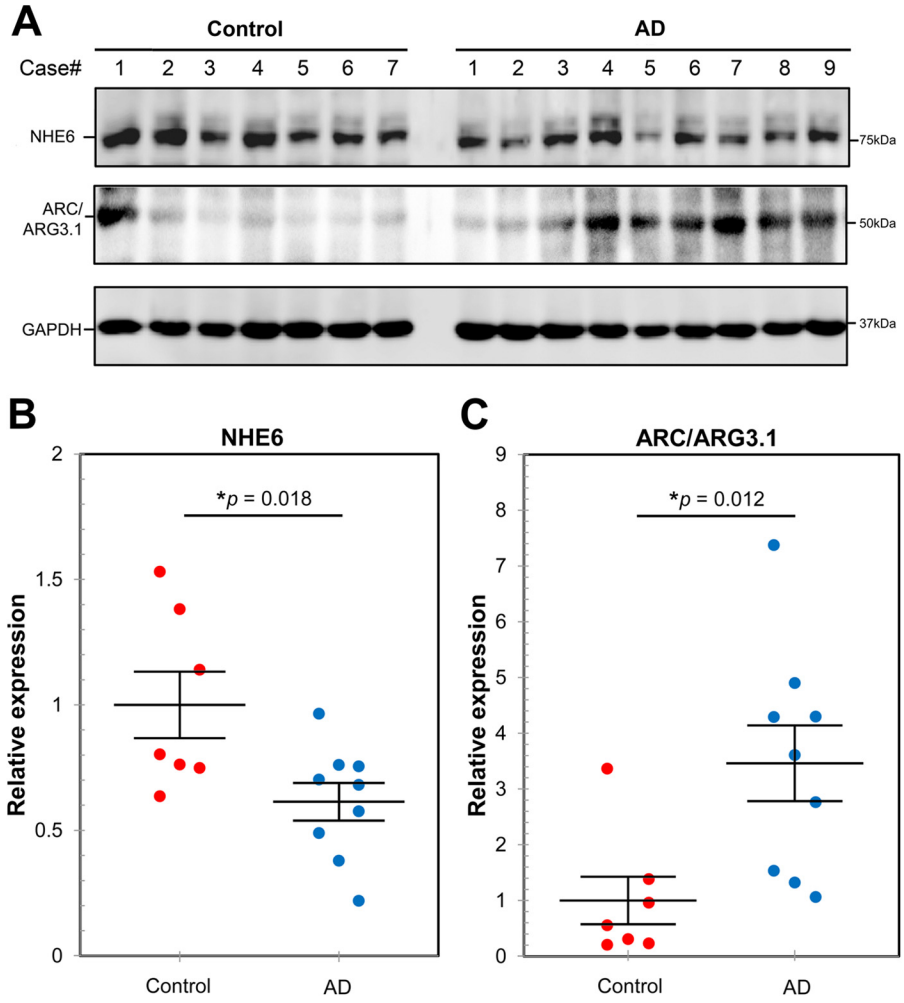

FIGURE 8. **Reduced NHE6 protein expression in Alzheimer disease brains.** *A*, Western blot of NHE6 and activity-regulated cytoskeleton-associated (Arc) protein in samples of gray matter from the medial frontal cortex of brains from AD patients compared with age-matched controls. Patient data are shown in Table 3. Shown is quantitation of NHE6 (*B*) and Arc (*C*) relative to GAPDH, used as a loading control (control, $n = 7$; AD patients, $n = 9$; *, $p < 0.05$; two-tailed *t* test). *Error bars*, S.E.

Pearson correlation coefficient, 0.86). Similarly, we had previously noted clustering of NHE6 (*SLC9A6*) with NRXN1 and other synapse genes expressed during normal brain development (1). In contrast, NHE6 expression did not correlate with average expression of 20 synapse genes up-regulated in AD in the data set of Blalock *et al.* (50, 57) (Fig. 7*H*).

To confirm and extend our observations from microarray studies, we compared expression of NHE6 protein in gray matter punch samples of medial frontal cortex from autopsies of patients with clinically and neuropathologically classified AD *versus* samples from age-matched controls (Fig. 8*A* and Table 3). We chose this brain region because medial frontal cortex is used in both Braak and CERAD staging as representative neocortex and is commonly affected in AD. NHE6 protein levels were significantly reduced in AD brains relative to control (Fig. 8*B*), consistent with down-regulation of NHE6 transcript observed in a microarray of AD brains. We note that Na^+/H^+ exchangers are estimated to have high transport rates of ~1,500 ions/s (58), so that even small changes may be functionally significant. We observed no changes in levels of loading control GAPDH protein between AD and control brains. For comparison, we examined the expression of activity-regulated cytoskeleton-associated (Arc) protein, a neuronal AD-linked protein known to be involved in endosomal mechanisms (59). It is worth noting that both NHE6 and Arc have been previously linked to autism and Angelman syndrome (16, 60). The levels of Arc protein were elevated in AD samples, consistent with previous findings (59) (Fig. 8*C*). Taken together with the functional link between endosomal pH and Aβ generation, these observations suggest that NHE6 may be a potential risk factor in the etiology of AD.

DISCUSSION

Emerging Links between NHE and AD—Phylogenetic clustering by Brett *et al.* (61) placed three intracellular NHE isoforms (NHE6, NHE7, and NHE9) in one distinct clade, separate from plasma membrane transporters (NHE1–5). Notably, all three members of the endosomal/TGN clade have since been linked to neurodegenerative disorders, consistent with overlapping yet distinct functions. We propose that intracellular NHE isoforms are non-redundant and are likely to differ in one or more of the following: (*a*) brain temporal and spatial expression patterns, (*b*) precise subcellular distribution, (*c*) transport function, and (*d*) interacting partners and regulation (1). X-linked

TABLE 3
Clinical and histopathological data for cases used in this study
F, female; M, male; W, white; B, black; PMD, post-mortem delay; BRC no., JHU Brain Resource Center code; NA, not applicable.

Case	Gender	Age	Race	PMD	CERAD	Braak's neurofibrillary staging	BRC no.
		years		*h*			
Control							
1	M	88	W	10	0	NA	631
2	M	73	W	9	0	NA	705
3	F	83	W	8	0	NA	718
4	M	59	W	12	0	NA	995
5	M	94	W	16	0	NA	1591
6	F	91	W	8	0	NA	1683
7	M	95	W	17	0	NA	2066
AD							
1	M	92	W	7	C	IV	1712
2	F	80	W	6.5	C	VI	1778
3	F	87	B	15.5	C	VI	1823
4	M	85	W	3.5	C	VI	1870
5	M	79	W	10.5	C	V	1898
6	F	84	W	5	C	V	1908
7	F	72	W	19	C	VI	1935
8	M	92	W	12	C	VI	1973
9	F	85	W	18	C	VI	2041

mutations in NHE6 cause Christianson syndrome, characterized by loss of neurons and glia, massive atrophy of cerebellum, and Tau pathologies (16, 18, 62). In a study aimed at understanding age-related cognitive changes in the human brain, the NHE6 transcript was found to be significantly down-regulated in aged neocortical areas important for cognitive functions, memory, speech production, and language understanding (association cortex, Broca and Wernicke areas) (63). Although the gene for NHE6 (*SLC9A6*) has not been linked to AD by genome-wide association studies, the closely related genes *SLC9A7* (NHE7) and *SLC9A9* (NHE9) have recently been identified as risk factors. NHE7 has been identified as a novel late onset Alzheimer disease risk gene through analyses of neuroimaging AD phenotypes and single nucleotide polymorphism (SNP) genetic variants (26). Furthermore, SNPs in NHE9 have been associated with (*a*) late onset Alzheimer disease and (*b*) response to cholinesterase inhibitor treatment in AD (25, 64). More recently, significant association between NHE9 variants and Alzheimer disease was identified in meta-analysis of a large genome-wide association study data set including ~5000 individuals (65). Collectively, emerging genetic, molecular, and histopathological evidence points to the TGN/endosomal NHE isoforms as potential risk factors for neurodegenerative diseases.

Vesicle Trafficking Dysfunction in AD—Endosomal pathology is an understudied component of Alzheimer disease and a promising target for therapy. Well known pathological hallmarks of AD include extracellular amyloid plaques, composed of Aβ fragments, and intracellular neurofibrillary tangles of the microtubule-binding protein Tau (66). However, these lesions appear later in disease progression, and efforts are under way to identify initial, treatable signs of dysfunction in AD. APP processing occurs within endosomal/TGN compartments by the sequential action of BACE1 and γ-secretase (Fig. 9). Enlarged endosomes are one of the earliest cellular phenotypes associated with AD, correlating with up-regulation of Rab proteins (8). Familial, AD-linked mutations in the γ-secretase subunit PS1 led to retention of APP within TGN compartments and increased cleavage (67), whereas silencing retromer subunits blocked retrograde transport of APP to decrease cleavage (40). Furthermore, exosomal secretion of Tau occurs early in AD and is thought to contribute to disease progression (68). These and many other data have been consolidated into a unifying hypothesis centering on vesicle trafficking dysfunction in AD. In this context, our demonstration that NHE6 alters APP processing implicates endosomal pH as an important modulator of amyloidogenic Aβ production and potentially of Tau aberrations (66). Notably, NHE6 deletion in mice leads to cellular phenotypes reminiscent of AD, including endosomal-lysosomal dysfunction, accumulation of unesterified cholesterol in endosomes, and neurodegeneration (69), although amyloidogenesis remains to be evaluated. Therefore, corroboration of our cell culture findings in the mouse model of *nhe6*^{KO} is warranted. There is growing interest in associations between neurodevelopmental and neurodegenerative disorders. Based on our data, we propose that enhanced amyloidogenic processing of APP may contribute to autism phenotypes seen in patients with NHE6 mutations. Given that NHE6 is a relatively new candidate gene for autism and intellectual disability, it is imperative to determine whether a subset of autists with deregulated NHE6 activity, either by loss-of-function mutations or by down-regulated gene expression, have a higher risk of premature aging and developing neurodegenerative disorders, such as Alzheimer disease.

Endosomal pH as a Therapeutic Target for Alzheimer Disease—Targeting the endosomal microenvironment to modulate activity of β- and γ-secretases has the advantage of avoiding toxicity ensuing from direct inhibition of these developmentally important enzymes. Luminal pH is set by a balance of pump and leak pathways from opposing proton transport by the V-ATPase and Na^+/H^+ exchanger (1) (Fig. 9). As we show here, increasing the leak pathway by NHE6 expression alkalinizes the endosomal lumen and limits Aβ production. It has long been appreciated that V-ATPase inhibitors (*e.g.* bafilomycin and concanamycin), alkalizing drugs (*e.g.* chloroquine and ammonium chloride), and ionophore drugs that

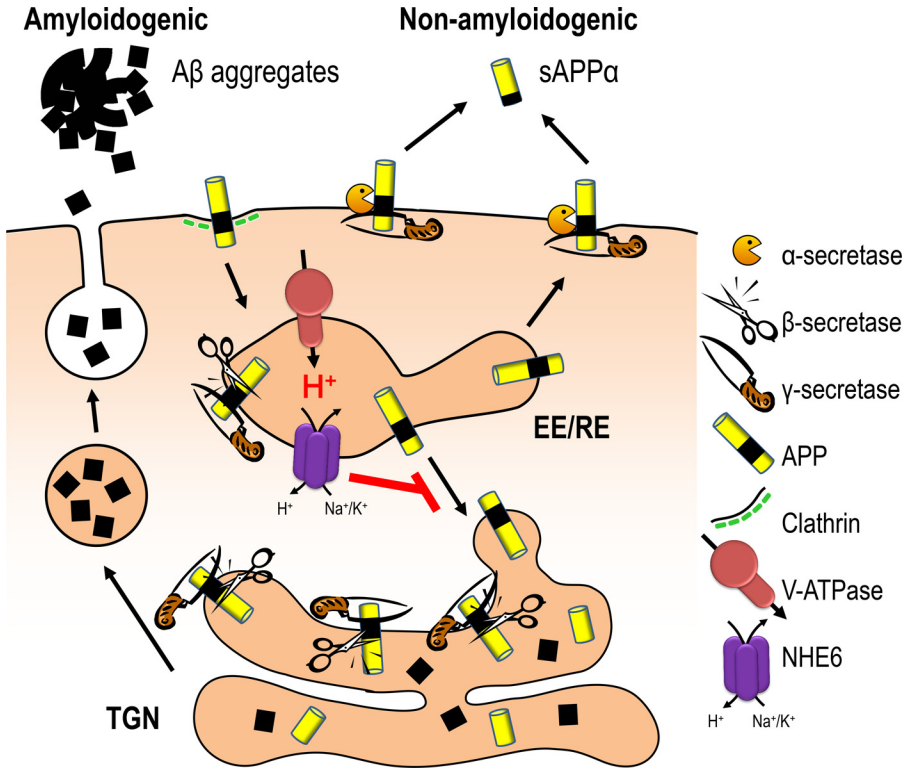

FIGURE 9. **Model for endosomal pH regulation of Aβ production.** APP can be consecutively cleaved by α- and γ-secretases (non-amyloidogenic pathway), mainly at the cell surface. Alternatively, APP is internalized by clathrin-mediated endocytosis to reach endosomes and the *trans*-Golgi network, where it undergoes amyloidogenic processing by β- and γ-secretases. Endosomal pH is precisely tuned by a balance of proton pumping (acidification) through the V-ATPase and proton leak (alkalization) via NHE6. NHE6 expression alkalinizes the endosomal lumen, blocks trafficking of APP from the endosome to TGN, and limits Aβ production.

mediate $Na^+(K^+)/H^+$ exchange (*e.g.* monensin and nigericin) alter APP processing and Aβ production (46–49, 70–72). Alkalization of endosomes could, at least in part, underlie APP redistribution seen in retromer/VPS35-depleted cells (40), given our observations that VPS35 deletion in yeast results in alkaline luminal pH (6). Furthermore, endosomal alkalization might explain APP redistribution and reduced Aβ production reported in APP stable cells treated with destruxin E, a V-ATPase inhibitor (45). However, V-ATPase inhibitors, alkalinizing drugs, and ionophores exert potent and multiple compartmental effects and have unwanted changes in vesicle trafficking and lysosomal function and have not been exploited for AD therapy thus far. We suggest that therapeutic elevation of endosomal pH using mildly alkalinizing drugs or by enhancing NHE6 activity will significantly reduce amyloid and Tau pathologies. For example, the weak bases bepridil and amiodarone, already in clinical use as calcium antagonists, were shown to mildly alkalinize endosomes and inhibit cleavage by β-secretase in cultured cells, in neurons, and in an *in vivo* guinea pig model (73). Membrane transporters like NHE6 are eminently "druggable targets" for Alzheimer disease and other neurological disorders that share endosomal dysfunction and trafficking defects. Given the success with discovery of small molecule potentiators for membrane transporters, such as CFTR, NHE6 could be an attractive therapeutic candidate to develop drugs to exert compartment-selective effects on luminal pH and minimize unwanted changes in vesicle function and trafficking.

Acknowledgments—We thank Drs. Meifang Xiao, Paul Worley, Juan C. Troncoso, and Philip Wong (Johns Hopkins University) for providing brain tissue samples and antibody and Drs. Svetlana Lutsenko (Johns Hopkins University) and Randy Schekman (University of California, Berkeley, CA) for providing cell lines. We gratefully acknowledge the technical assistance and comments of Dr. Yuta Hatori and Ya-Wen Lu (Johns Hopkins University).

REFERENCES

1. Kondapalli, K. C., Prasad, H., and Rao, R. (2014) An inside job: how endosomal Na^+/H^+ exchangers link to autism and neurological disease. *Front. Cell Neurosci.* **8,** 172
2. Brett, C. L., Wei, Y., Donowitz, M., and Rao, R. (2002) Human Na^+/H^+ exchanger isoform 6 is found in recycling endosomes of cells, not in mitochondria. *Am. J. Physiol. Cell Physiol.* **282,** C1031–C1041
3. Brett, C. L., Tukaye, D. N., Mukherjee, S., and Rao, R. (2005) The yeast endosomal Na+K+/H+ exchanger Nhx1 regulates cellular pH to control vesicle trafficking. *Mol. Biol. Cell* **16,** 1396–1405
4. Nass, R., and Rao, R. (1998) Novel localization of a Na^+/H^+ exchanger in a late endosomal compartment of yeast: implications for vacuole biogenesis. *J. Biol. Chem.* **273,** 21054–21060
5. Bowers, K., Levi, B. P., Patel, F. I., and Stevens, T. H. (2000) The sodium/proton exchanger Nhx1p is required for endosomal protein trafficking in the yeast *Saccharomyces cerevisiae*. *Mol. Biol. Cell* **11,** 4277–4294
6. Brett, C. L., Kallay, L., Hua, Z., Green, R., Chyou, A., Zhang, Y., Graham, T. R., Donowitz, M., and Rao, R. (2011) Genome-wide analysis reveals the vacuolar pH-stat of *Saccharomyces cerevisiae*. *PLoS One* **6,** e17619
7. Wolfe, D. M., Lee, J. H., Kumar, A., Lee, S., Orenstein, S. J., and Nixon, R. A. (2013) Autophagy failure in Alzheimer's disease and the role of defective lysosomal acidification. *Eur. J. Neurosci.* **37,** 1949–1961
8. Cataldo, A. M., Mathews, P. M., Boiteau, A. B., Hassinger, L. C., Peterhoff,

C. M., Jiang, Y., Mullaney, K., Neve, R. L., Gruenberg, J., and Nixon, R. A. (2008) Down syndrome fibroblast model of Alzheimer-related endosome pathology: accelerated endocytosis promotes late endocytic defects. *Am. J. Pathol.* **173,** 370–384
9. Karch, C. M., and Goate, A. M. (2015) Alzheimer's disease risk genes and mechanisms of disease pathogenesis. *Biol. Psychiatry* **77,** 43–51
10. Das, U., Scott, D. A., Ganguly, A., Koo, E. H., Tang, Y., and Roy, S. (2013) Activity-induced convergence of APP and BACE-1 in acidic microdomains via an endocytosis-dependent pathway. *Neuron* **79,** 447–460
11. Vassar, R., Bennett, B. D., Babu-Khan, S., Kahn, S., Mendiaz, E. A., Denis, P., Teplow, D. B., Ross, S., Amarante, P., Loeloff, R., Luo, Y., Fisher, S., Fuller, J., Edenson, S., Lile, J., Jarosinski, M. A., Biere, A. L., Curran, E., Burgess, T., Louis, J. C., Collins, F., Treanor, J., Rogers, G., and Citron, M. (1999) β-secretase cleavage of Alzheimer's amyloid precursor protein by the transmembrane aspartic protease BACE. *Science* **286,** 735–741
12. Cai, H., Wang, Y., McCarthy, D., Wen, H., Borchelt, D. R., Price, D. L., and Wong, P. C. (2001) BACE1 is the major β-secretase for generation of Aβ peptides by neurons. *Nat. Neurosci.* **4,** 233–234
13. Olubiyi, O. O., and Strodel, B. (2012) Structures of the amyloid β-peptides Aβ1–40 and Aβ1–42 as influenced by pH and a D-peptide. *J. Phys. Chem. B* **116,** 3280–3291
14. Caglayan, S., Takagi-Niidome, S., Liao, F., Carlo, A. S., Schmidt, V., Burgert, T., Kitago, Y., Füchtbauer, E. M., Füchtbauer, A., Holtzman, D. M., Takagi, J., and Willnow, T. E. (2014) Lysosomal sorting of amyloid-β by the SORLA receptor is impaired by a familial Alzheimer's disease mutation. *Sci. Transl. Med.* **6,** 223ra20
15. Tarpey, P. S., Smith, R., Pleasance, E., Whibley, A., Edkins, S., Hardy, C., O'Meara, S., Latimer, C., Dicks, E., Menzies, A., Stephens, P., Blow, M., Greenman, C., Xue, Y., Tyler-Smith, C., Thompson, D., Gray, K., Andrews, J., Barthorpe, S., Buck, G., Cole, J., Dunmore, R., Jones, D., Maddison, M., Mironenko, T., Turner, R., Turrell, K., Varian, J., West, S., Widaa, S., Wray, P., Teague, J., Butler, A., Jenkinson, A., Jia, M., Richardson, D., Shepherd, R., Wooster, R., Tejada, M. I., Martinez, F., Carvill, G., Goliath, R., de Brouwer, A. P., van Bokhoven, H., Van Esch, H., Chelly, J., Raynaud, M., Ropers, H. H., Abidi, F. E., Srivastava, A. K., Cox, J., Luo, Y., Mallya, U., Moon, J., Parnau, J., Mohammed, S., Tolmie, J. L., Shoubridge, C., Corbett, M., Gardner, A., Haan, E., Rujirabanjerd, S., Shaw, M., Vandeleur, L., Fullston, T., Easton, D. F., Boyle, J., Partington, M., Hackett, A., Field, M., Skinner, C., Stevenson, R. E., Bobrow, M., Turner, G., Schwartz, C. E., Gecz, J., Raymond, F. L., Futreal, P. A., and Stratton, M. R. (2009) A systematic, large-scale resequencing screen of X-chromosome coding exons in mental retardation. *Nat. Genet.* **41,** 535–543
16. Gilfillan, G. D., Selmer, K. K., Roxrud, I., Smith, R., Kyllerman, M., Eiklid, K., Kroken, M., Mattingsdal, M., Egeland, T., Stenmark, H., Sjøholm, H., Server, A., Samuelsson, L., Christianson, A., Tarpey, P., Whibley, A., Stratton, M. R., Futreal, P. A., Teague, J., Edkins, S., Gecz, J., Turner, G., Raymond, F. L., Schwartz, C., Stevenson, R. E., Undlien, D. E., and Strømme, P. (2008) SLC9A6 mutations cause X-linked mental retardation, microcephaly, epilepsy, and ataxia, a phenotype mimicking Angelman syndrome. *Am. J. Hum. Genet.* **82,** 1003–1010
17. Ouyang, Q., Lizarraga, S. B., Schmidt, M., Yang, U., Gong, J., Ellisor, D., Kauer, J. A., and Morrow, E. M. (2013) Christianson syndrome protein NHE6 modulates TrkB endosomal signaling required for neuronal circuit development. *Neuron* **80,** 97–112
18. Garbern, J. Y., Neumann, M., Trojanowski, J. Q., Lee, V. M., Feldman, G., Norris, J. W., Friez, M. J., Schwartz, C. E., Stevenson, R., and Sima, A. A. (2010) A mutation affecting the sodium/proton exchanger, SLC9A6, causes mental retardation with tau deposition. *Brain* **133,** 1391–1402
19. Schwede, M., Garbett, K., Mirnics, K., Geschwind, D. H., and Morrow, E. M. (2014) Genes for endosomal NHE6 and NHE9 are misregulated in autism brains. *Mol. Psychiatry* **19,** 277–279
20. Vos, S. J., Xiong, C., Visser, P. J., Jasielec, M. S., Hassenstab, J., Grant, E. A., Cairns, N. J., Morris, J. C., Holtzman, D. M., and Fagan, A. M. (2013) Preclinical Alzheimer's disease and its outcome: a longitudinal cohort study. *Lancet Neurol.* **12,** 957–965
21. Wegiel, J., Frackowiak, J., Mazur-Kolecka, B., Schanen, N. C., Cook, E. H., Jr., Sigman, M., Brown, W. T., Kuchna, I., Wegiel, J., Nowicki, K., Imaki, H., Ma, S. Y., Chauhan, A., Chauhan, V., Miller, D. L., Mehta, P. D., Flory, M., Cohen, I. L., London, E., Reisberg, B., de Leon, M. J., and Wisniewski, T. (2012) Abnormal intracellular accumulation and extracellular Aβ deposition in idiopathic and Dup15q11.2-q13 autism spectrum disorders. *PLoS One* **7,** e35414
22. Westmark, C. J., and Malter, J. S. (2007) FMRP mediates mGluR5-dependent translation of amyloid precursor protein. *PLoS Biol.* **5,** e52
23. Sokol, D. K., Chen, D., Farlow, M. R., Dunn, D. W., Maloney, B., Zimmer, J. A., and Lahiri, D. K. (2006) High levels of Alzheimer β-amyloid precursor protein (APP) in children with severely autistic behavior and aggression. *J. Child Neurol.* **21,** 444–449
24. Hauser, M. A., Li, Y. J., Xu, H., Noureddine, M. A., Shao, Y. S., Gullans, S. R., Scherzer, C. R., Jensen, R. V., McLaurin, A. C., Gibson, J. R., Scott, B. L., Jewett, R. M., Stenger, J. E., Schmechel, D. E., Hulette, C. M., and Vance, J. M. (2005) Expression profiling of substantia nigra in Parkinson disease, progressive supranuclear palsy, and frontotemporal dementia with parkinsonism. *Arch. Neurol.* **62,** 917–921
25. Martinelli-Boneschi, F., Giacalone, G., Magnani, G., Biella, G., Coppi, E., Santangelo, R., Brambilla, P., Esposito, F., Lupoli, S., Clerici, F., Benussi, L., Ghidoni, R., Galimberti, D., Squitti, R., Confaloni, A., Bruno, G., Pichler, S., Mayhaus, M., Riemenschneider, M., Mariani, C., Comi, G., Scarpini, E., Binetti, G., Forloni, G., Franceschi, M., and Albani, D. (2013) Pharmacogenomics in Alzheimer's disease: a genome-wide association study of response to cholinesterase inhibitors. *Neurobiol. Aging* 10.1016/j.neurobiolaging.2012.12.008
26. Meda, S. A., Narayanan, B., Liu, J., Perrone-Bizzozero, N. I., Stevens, M. C., Calhoun, V. D., Glahn, D. C., Shen, L., Risacher, S. L., Saykin, A. J., and Pearlson, G. D. (2012) A large scale multivariate parallel ICA method reveals novel imaging-genetic relationships for Alzheimer's disease in the ADNI cohort. *Neuroimage* **60,** 1608–1621
27. Encinas, M., Iglesias, M., Liu, Y., Wang, H., Muhaisen, A., Ceña, V., Gallego, C., and Comella, J. X. (2000) Sequential treatment of SH-SY5Y cells with retinoic acid and brain-derived neurotrophic factor gives rise to fully differentiated, neurotrophic factor-dependent, human neuron-like cells. *J. Neurochem.* **75,** 991–1003
28. Kondapalli, K. C., Hack, A., Schushan, M., Landau, M., Ben-Tal, N., and Rao, R. (2013) Functional evaluation of autism-associated mutations in NHE9. *Nat. Commun.* **4,** 2510
29. Kim, M. K., Min, D. J., Rabin, M., and Licht, J. D. (2011) Functional characterization of Wilms tumor-suppressor WTX and tumor-associated mutants. *Oncogene* **30,** 832–842
30. Vetrivel, K. S., Meckler, X., Chen, Y., Nguyen, P. D., Seidah, N. G., Vassar, R., Wong, P. C., Fukata, M., Kounnas, M. Z., and Thinakaran, G. (2009) Alzheimer disease Abeta production in the absence of S-palmitoylation-dependent targeting of BACE1 to lipid rafts. *J. Biol. Chem.* **284,** 3793–3803
31. Deane, E. C., Ilie, A. E., Sizdahkhani, S., Das Gupta, M., Orlowski, J., and McKinney, R. A. (2013) Enhanced recruitment of endosomal Na^+/H^+ exchanger NHE6 into dendritic spines of hippocampal pyramidal neurons during NMDA receptor-dependent long-term potentiation. *J. Neurosci.* **33,** 595–610
32. Demars, M., Hu, Y. S., Gadadhar, A., and Lazarov, O. (2010) Impaired neurogenesis is an early event in the etiology of familial Alzheimer's disease in transgenic mice. *J. Neurosci. Res.* **88,** 2103–2117
33. Zhang, B., Gaiteri, C., Bodea, L. G., Wang, Z., McElwee, J., Podtelezhnikov, A. A., Zhang, C., Xie, T., Tran, L., Dobrin, R., Fluder, E., Clurman, B., Melquist, S., Narayanan, M., Suver, C., Shah, H., Mahajan, M., Gillis, T., Mysore, J., MacDonald, M. E., Lamb, J. R., Bennett, D. A., Molony, C., Stone, D. J., Gudnason, V., Myers, A. J., Schadt, E. E., Neumann, H., Zhu, J., and Emilsson, V. (2013) Integrated systems approach identifies genetic nodes and networks in late-onset Alzheimer's disease. *Cell* **153,** 707–720
34. Kohn, K. W., Zeeberg, B. M., Reinhold, W. C., and Pommier, Y. (2014) Gene expression correlations in human cancer cell lines define molecular interaction networks for epithelial phenotype. *PLoS One* **9,** e99269
35. Hardy, J., Bogdanovic, N., Winblad, B., Portelius, E., Andreasen, N., Cedazo-Minguez, A., and Zetterberg, H. (2014) Pathways to Alzheimer's disease. *J. Intern. Med.* **275,** 296–303
36. DeMattos, R. B., Cirrito, J. R., Parsadanian, M., May, P. C., O'Dell, M. A., Taylor, J. W., Harmony, J. A., Aronow, B. J., Bales, K. R., Paul, S. M., and Holtzman, D. M. (2004) ApoE and clusterin cooperatively suppress Aβ

levels and deposition: evidence that ApoE regulates extracellular Aβ metabolism *in vivo*. *Neuron* **41,** 193–202
37. Malik, M., Simpson, J. F., Parikh, I., Wilfred, B. R., Fardo, D. W., Nelson, P. T., and Estus, S. (2013) CD33 Alzheimer's risk-altering polymorphism, CD33 expression, and exon 2 splicing. *J. Neurosci.* **33,** 13320–13325
38. Kanatsu, K., Morohashi, Y., Suzuki, M., Kuroda, H., Watanabe, T., Tomita, T., and Iwatsubo, T. (2014) Decreased CALM expression reduces Aβ42 to total Aβ ratio through clathrin-mediated endocytosis of γ-secretase. *Nat. Commun.* **5,** 3386
39. König, G., Masters, C. L., and Beyreuther, K. (1990) Retinoic acid induced differentiated neuroblastoma cells show increased expression of the β A4 amyloid gene of Alzheimer's disease and an altered splicing pattern. *FEBS Lett.* **269,** 305–310
40. Choy, R. W., Cheng, Z., and Schekman, R. (2012) Amyloid precursor protein (APP) traffics from the cell surface via endosomes for amyloid beta (Abeta) production in the *trans*-Golgi network. *Proc. Natl. Acad. Sci. U.S.A.* **109,** E2077–E2082
41. Nyasae, L. K., Schell, M. J., and Hubbard, A. L. (2014) Copper directs ATP7B to the apical domain of hepatic cells via basolateral endosomes. *Traffic* **15,** 1344–1365
42. Mollenhauer, H. H., Morré, D. J., and Rowe, L. D. (1990) Alteration of intracellular traffic by monensin; mechanism, specificity and relationship to toxicity. *Biochim. Biophys. Acta* **1031,** 225–246
43. Muro, S., Mateescu, M., Gajewski, C., Robinson, M., Muzykantov, V. R., and Koval, M. (2006) Control of intracellular trafficking of ICAM-1-targeted nanocarriers by endothelial Na^+/H^+ exchanger proteins. *Am. J. Physiol. Lung Cell. Mol. Physiol.* **290,** L809–L817
44. Xinhan, L., Matsushita, M., Numaza, M., Taguchi, A., Mitsui, K., and Kanazawa, H. (2011) Na^+/H^+ exchanger isoform 6 (NHE6/SLC9A6) is involved in clathrin-dependent endocytosis of transferrin. *Am. J. Physiol. Cell Physiol.* **301,** C1431–C1444
45. Itoh, N., Okochi, M., Tagami, S., Nishitomi, K., Nakayama, T., Yanagida, K., Fukumori, A., Jiang, J., Mori, K., Hosono, M., Kikuchi, J., Nakano, Y., Takinami, Y., Dohi, K., Nishigaki, A., Takemoto, H., Minagawa, K., Katoh, T., Willem, M., Haass, C., Morihara, T., Tanaka, T., Kudo, T., Hasegawa, H., Nishimura, M., Sakaguchi, G., Kato, A., and Takeda, M. (2009) Destruxin E decreases β-amyloid generation by reducing colocalization of β-amyloid-cleaving enzyme 1 and β-amyloid protein precursor. *Neurodegener. Dis.* **6,** 230–239
46. Caporaso, G. L., Gandy, S. E., Buxbaum, J. D., and Greengard, P. (1992) Chloroquine inhibits intracellular degradation but not secretion of Alzheimer β/A4 amyloid precursor protein. *Proc. Natl. Acad. Sci. U.S.A.* **89,** 2252–2256
47. Wolozin, B., Bacic, M., Merrill, M. J., Lesch, K. P., Chen, C., Lebovics, R. S., and Sunderland, T. (1992) Differential expression of carboxyl terminal derivatives of amyloid precursor protein among cell lines. *J. Neurosci. Res.* **33,** 163–169
48. Lahiri, D. K. (1994) Effect of ionophores on the processing of the β-amyloid precursor protein in different cell lines. *Cell. Mol. Neurobiol.* **14,** 297–313
49. Urmoneit, B., Turner, J., and Dyrks, T. (1998) Pulse-chase experiments revealed β-secretase cleavage from immature full-length amyloid precursor protein harboring the Swedish mutation: implications for distinct pathways. *J. Mol. Neurosci.* **11,** 141–150
50. Blalock, E. M., Geddes, J. W., Chen, K. C., Porter, N. M., Markesbery, W. R., and Landfield, P. W. (2004) Incipient Alzheimer's disease: microarray correlation analyses reveal major transcriptional and tumor suppressor responses. *Proc. Natl. Acad. Sci. U.S.A.* **101,** 2173–2178
51. Dunckley, T., Beach, T. G., Ramsey, K. E., Grover, A., Mastroeni, D., Walker, D. G., LaFleur, B. J., Coon, K. D., Brown, K. M., Caselli, R., Kukull, W., Higdon, R., McKeel, D., Morris, J. C., Hulette, C., Schmechel, D., Reiman, E. M., Rogers, J., and Stephan, D. A. (2006) Gene expression correlates of neurofibrillary tangles in Alzheimer's disease. *Neurobiol. Aging* **27,** 1359–1371
52. Liang, W. S., Dunckley, T., Beach, T. G., Grover, A., Mastroeni, D., Walker, D. G., Caselli, R. J., Kukull, W. A., McKeel, D., Morris, J. C., Hulette, C., Schmechel, D., Alexander, G. E., Reiman, E. M., Rogers, J., and Stephan, D. A. (2007) Gene expression profiles in anatomically and functionally distinct regions of the normal aged human brain. *Physiol. Genomics* **28,** 311–322
53. Nunez-Iglesias, J., Liu, C. C., Morgan, T. E., Finch, C. E., and Zhou, X. J. (2010) Joint genome-wide profiling of miRNA and mRNA expression in Alzheimer's disease cortex reveals altered miRNA regulation. *PLoS One* **5,** e8898
54. O'Brien, R. J., and Wong, P. C. (2011) Amyloid precursor protein processing and Alzheimer's disease. *Annu. Rev. Neurosci.* **34,** 185–204
55. Wang, Z., Yang, L., and Zheng, H. (2012) Role of APP and Aβ in synaptic physiology. *Curr. Alzheimer Res.* **9,** 217–226
56. Frost, B., Götz, J., and Feany, M. B. (2015) Connecting the dots between tau dysfunction and neurodegeneration. *Trends Cell Biol.* **25,** 46–53
57. Gómez Ravetti, M., Rosso, O. A., Berretta, R., and Moscato, P. (2010) Uncovering molecular biomarkers that correlate cognitive decline with the changes of hippocampus' gene expression profiles in Alzheimer's disease. *PLoS One* **5,** e10153
58. Lee, C., Kang, H. J., von Ballmoos, C., Newstead, S., Uzdavinys, P., Dotson, D. L., Iwata, S., Beckstein, O., Cameron, A. D., and Drew, D. (2013) A two-domain elevator mechanism for sodium/proton antiport. *Nature* **501,** 573–577
59. Wu, J., Petralia, R. S., Kurushima, H., Patel, H., Jung, M. Y., Volk, L., Chowdhury, S., Shepherd, J. D., Dehoff, M., Li, Y., Kuhl, D., Huganir, R. L., Price, D. L., Scannevin, R., Troncoso, J. C., Wong, P. C., and Worley, P. F. (2011) Arc/Arg3.1 regulates an endosomal pathway essential for activity-dependent β-amyloid generation. *Cell* **147,** 615–628
60. Greer, P. L., Hanayama, R., Bloodgood, B. L., Mardinly, A. R., Lipton, D. M., Flavell, S. W., Kim, T. K., Griffith, E. C., Waldon, Z., Maehr, R., Ploegh, H. L., Chowdhury, S., Worley, P. F., Steen, J., and Greenberg, M. E. (2010) The Angelman Syndrome protein Ube3A regulates synapse development by ubiquitinating arc. *Cell* **140,** 704–716
61. Brett, C. L., Donowitz, M., and Rao, R. (2005) Evolutionary origins of eukaryotic sodium/proton exchangers. *Am. J. Physiol. Cell Physiol.* **288,** C223–239
62. Christianson, A. L., Stevenson, R. E., van der Meyden, C. H., Pelser, J., Theron, F. W., van Rensburg, P. L., Chandler, M., and Schwartz, C. E. (1999) X linked severe mental retardation, craniofacial dysmorphology, epilepsy, ophthalmoplegia, and cerebellar atrophy in a large South African kindred is localised to Xq24-q27. *J. Med. Genet.* **36,** 759–766
63. Naumova, O. Y., Palejev, D., Vlasova, N. V., Lee, M., Rychkov, S. Y., Babich, O. N., M. Vaccarino, F., and Grigorenko, E. L. (2012) Age-related changes of gene expression in the neocortex: preliminary data on RNA-Seq of the transcriptome in three functionally distinct cortical areas. *Dev. Psychopathol.* **24,** 1427–1442
64. Coelho, L., Goertzel, B., Pennachin, C., and Heward, C. (2010) Classifier ensemble based analysis of a genome-wide SNP dataset concerning late-onset Alzheimer disease. *Int. J. Software Sci. Comput. Intell.* 10.4018/jssci.2010100105
65. Pérez-Palma, E., Bustos, B. I., Villamán, C. F., Alarcón, M. A., Avila, M. E., Ugarte, G. D., Reyes, A. E., Opazo, C., De Ferrari, G. V., Alzheimer's Disease Neuroimaging Initiative, and NIA-LOAD/NCRAD Family Study Group (2014) Overrepresentation of glutamate signaling in Alzheimer's disease: network-based pathway enrichment using meta-analysis of genome-wide association studies. *PloS One* **9,** e95413
66. Funk, K. E., and Kuret, J. (2012) Lysosomal fusion dysfunction as a unifying hypothesis for Alzheimer's disease pathology. *Int. J. Alzheimers Dis.* **2012,** 752894
67. Cai, D., Leem, J. Y., Greenfield, J. P., Wang, P., Kim, B. S., Wang, R., Lopes, K. O., Kim, S. H., Zheng, H., Greengard, P., Sisodia, S. S., Thinakaran, G., and Xu, H. (2003) Presenilin-1 regulates intracellular trafficking and cell surface delivery of β-amyloid precursor protein. *J. Biol. Chem.* **278,** 3446–3454
68. Saman, S., Kim, W., Raya, M., Visnick, Y., Miro, S., Saman, S., Jackson, B., McKee, A. C., Alvarez, V. E., Lee, N. C., and Hall, G. F. (2012) Exosome-associated tau is secreted in tauopathy models and is selectively phosphorylated in cerebrospinal fluid in early Alzheimer disease. *J. Biol. Chem.* **287,** 3842–3849
69. Strømme, P., Dobrenis, K., Sillitoe, R. V., Gulinello, M., Ali, N. F., Davidson, C., Micsenyi, M. C., Stephney, G., Ellevog, L., Klungland, A., and

Walkley, S. U. (2011) X-linked Angelman-like syndrome caused by Slc9a6 knockout in mice exhibits evidence of endosomal-lysosomal dysfunction. *Brain* **134,** 3369–3383
70. Haass, C., Capell, A., Citron, M., Teplow, D. B., and Selkoe, D. J. (1995) The vacuolar H^+-ATPase inhibitor bafilomycin A1 differentially affects proteolytic processing of mutant and wild-type β-amyloid precursor protein. *J. Biol. Chem.* **270,** 6186–6192
71. Knops, J., Suomensaari, S., Lee, M., McConlogue, L., Seubert, P., and Sinha, S. (1995) Cell-type and amyloid precursor protein-type specific inhibition of A β release by bafilomycin A1, a selective inhibitor of vacuolar ATPases. *J. Biol. Chem.* **270,** 2419–2422
72. Schrader-Fischer, G., and Paganetti, P. A. (1996) Effect of alkalizing agents on the processing of the beta-amyloid precursor protein. *Brain Res.* **716,** 91–100
73. Mitterreiter, S., Page, R. M., Kamp, F., Hopson, J., Winkler, E., Ha, H. R., Hamid, R., Herms, J., Mayer, T. U., Nelson, D. J., Steiner, H., Stahl, T., Zeitschel, U., Rossner, S., Haass, C., and Lichtenthaler, S. F. (2010) Bepridil and amiodarone simultaneously target the Alzheimer's disease beta- and gamma-secretase via distinct mechanisms. *J. Neurosci.* **30,** 8974–8983
74. Yanai, I., Benjamin, H., Shmoish, M., Chalifa-Caspi, V., Shklar, M., Ophir, R., Bar-Even, A., Horn-Saban, S., Safran, M., Domany, E., Lancet, D., and Shmueli, O. (2005) Genome-wide midrange transcription profiles reveal expression level relationships in human tissue specification. *Bioinformatics* **21,** 650–659
75. Kojetin, D. J., Thompson, R. J., and Cavanagh, J. (2003) Sub-classification of response regulators using the surface characteristics of their receiver domains. *FEBS Lett.* **554,** 231–236